# Partons in nuclei

R. P. Bickerstaff,* M. C. Birse,† and G. A. Miller
*Institute for Nuclear Theory, Department of Physics, FM-15, University of Washington, Seattle, Washington 98195*
(Received 9 September 1985; revised manuscript received 4 February 1986)

We study the different explanations of the European Muon Collaboration effect. Although the theoretical models are very sensitive to input free-nucleon structure functions, we find that each has distinctive testable traits. Therefore, we examine different reactions to see which can distinguish the models. Deep-inelastic (anti)neutrino-nucleus scattering data are examined, but we find that the model differences to be exposed by this process are small. $J/\psi$ production in lepton-nucleus collision is, in principle, capable of determining the nuclear gluon distribution, but there are too many difficulties to successfully separate the different models. We find that the Drell-Yan process is better suited than antineutrino scattering to determine the nuclear ocean distributions. These may be studied in an experimentally accessible kinematic region in which a quark from the projectile annihilates with a nuclear antiquark.

## I. INTRODUCTION

Deep-inelastic lepton-nucleon scattering experiments probe the quark structure of nucleons and nuclei are the source of nucleons. It was long assumed that deep-inelastic scattering (DIS) on a nucleus of mass number $A$ was just an incoherent sum of scattering on $A$ nucleons. The recent observation that this is not quite true[1] provides both a dilemma and an opportunity. Much knowledge obtained from this nuclear data is now questionable. Furthermore, we are faced with explaining why the nuclear environment influences the character of a neutron or proton. Quark interactions in nuclei[2] may be important. To fully profit from this avenue of investigation one requires a unique explanation, but many quite different ones seem possible. Our goal is to suggest how some of these may be eliminated by means of additional experiments using other reactions.

Changes in the parton structure of nucleons in nuclei were first noticed by the European Muon Collaboration (EMC), when they compared the deep-inelastic scattering of muons from deuterium (where the nucleons are essentially free) and iron.[1] It was found that the structure function (per nucleon) of iron is significantly larger at small values of $x$ ($\lesssim 0.2$) and smaller at medium values of $x$ ($\sim 0.6$) than that of a free nucleon. This nuclear dependence has come to be known as the "EMC effect." Subsequent DIS experiments[3–6] with both muons and electrons have confirmed the medium-$x$ depletion both in iron and other nuclei but there is some doubt about the low-$x$ enhancement. Neutrino-nucleus DIS data,[7–10] while showing large errors, are consistent with the medium-$x$ depletion, but place further doubt on the low-$x$ enhancement, especially a substantial one such as seen by the EMC. Despite this uncertainty in the details of the experimental results, it seems clear that quark distribution functions do depend on the nuclear environment.

Most of the explanations of the EMC effect fall into one of three categories. The first involves conventional nuclear physics, employing only nucleonic and pionic degrees of freedom.[11–15] Another idea[16–23] is that nuclear wave functions contain significant components with six (or more) quark clusters. Still another class of explanations motivated by QCD (Refs. 24–27) is derived from the observation that the differences between the structure functions of different nuclei at fixed $Q^2$ imitate the $Q^2$ dependence of the distribution for a single target.

These three classes of models seem reasonable, but do not encompass every proposed mechanism for the EMC effect. See, for example, the antishadowing model of Nikolaev and Zakharov.[28]

One possibility for differentiating models might be to use the dependence of the quark distributions on the nuclear target ($A$ dependence). This does eliminate some early models;[29] however, as long as experimentally correct nuclear densities are used, each of the above classes of models can explain the $A$ dependence. Therefore, the goal of this paper is to explore possibilities of using probes other than muons or electrons to determine nuclear structure functions. We try to examine elementary processes where the impulse approximation is valid. To see if certain reactions can distinguish the models it is necessary to evaluate these carefully (Sec. II). We find that the predictions of each model depend significantly on the free-nucleon distribution function used as input. There are also other flaws in each of the models. However our basic result is that each model has qualitative testable features.

Deep-inelastic neutrino and antineutrino scattering allows separation of the quark and antiquark contributions. We compute nuclear structure functions for weak interactions, using each of the models and find that comparison with neutrino data fails to distinguish these (Sec. III). Each of the theoretical treatments is constrained by the results for charged-lepton DIS. As exposed by neutrino data, any remaining differences are small.

The purpose of nuclear $J/\psi$ production holds the promise of determining the nuclear gluon distribution. We find (Sec. IV) that only the third class of model allows for a significant gluonic $A$ dependence. However, the available data[30] are at small $x$ where there is considerable

 

leeway in the models and other problems abound.

Another possibility is to study lepton pairs produced in proton-nucleus collisions at high energy (Sec. V). This is the "Drell-Yan" process[31] of Fig. 1. The models of the nuclear quark distribution function also provide models of the nuclear antiquark distribution function. In Ref. 32 we found that differences between the predictions for the antiquark distributions are greatly enhanced in kinematic regions corresponding to valence quarks from the proton and antiquarks from the nucleus both having moderate to large $x$. Here we bolster that result by using more realistic kinematics, and making a full QCD calculation including gluon Compton scattering. Furthermore we find that one version of the nucleon-pion model[15] is not consistent with antiquark distributions extracted from Drell-Yan data. Some experimental questions are also addressed.

Thus we are left with the Drell-Yan process as the most promising reaction. A brief summary is given in Sec. VI.

## II. MODELS FOR NUCLEAR PARTON DISTRIBUTIONS

In this section we review the salient testable features of the three main classes of explanation: enhancement of the pionic components of nuclear wave functions, the presence of six- (or more-) quark clusters, or a rescaling of the momentum-transfer dependence of nuclear parton distributions. The sensitivity to the choice of free-nucleon structure functions is studied carefully.

It is necessary to mention a few details prior to beginning the task of evaluating models. Recall that deep-inelastic charged-lepton scattering measures the nucleon structure functions $F_{1,2}(x,Q^2)$ where the Bjorken scaling variable $x=Q^2/2m_N\nu$ is the same as the fraction $x=k^+/p_N^+$ of the nucleon's light front momentum carried by the struck parton. The energy transfer is $\nu$. See Wimpenny[33] for a review of the data. We display only the SLAC data[8] here.

Theoretical comparisons with DIS on nuclei are made by using medium-modified distributions $q^A(x,Q^2)$. To facilitate comparison between different nuclei we always use the distribution per nucleon. Hence our nuclear structure functions $F^A(x,Q^2)$ are structure functions per nucleon. For a nucleus, the natural scaling variable is $x_A=k^+/p_A^+$, the fraction of the momentum of the whole nucleus carried by the quark in question. However, for purposes of comparing different nuclei, we continue to use the Bjorken variable $x=x_A M_A/m_N$, which ranges in value from 0 to about $A$.

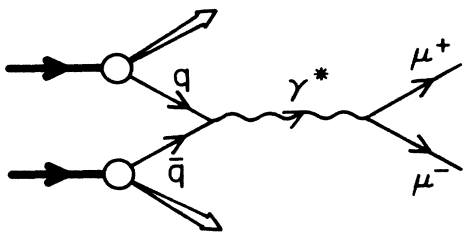


FIG. 1. The basic Drell-Yan process.

### A. Nucleons and pions

From the point of view of ordinary nuclear-structure physics, the low-momentum nuclear wave function is described purely in terms of hadronic degrees of freedom: nucleons, pions, and possibly deltas. The quark substructure plays a role only in the high-momentum-transfer processes (DIS, Drell-Yan, etc.).

The nuclear binding comes about by the exchange of pions and other mesons. The resulting electromagnetic structure function per nucleon may be described by[11]

$$F_2^A(x,Q^2)=\int_x^A dz\, f_N^A(z)F_2^N\left[\frac{x}{z},Q^2\right] + \int_x^A dy\, f_\pi^A(y)F_2^\pi\left[\frac{x}{y},Q^2\right], \tag{2.1}$$

where $f_N^A$ is the momentum distribution of nucleons within a nucleus with mass number $A$, $F_2^N$ is the free-nucleon structure function, $f_\pi^A$ is the distribution of excess pions contributing to DIS, and $F_2^\pi$ is the pion structure function.

The first term of Eq. (2.1) describes the influence of the nucleon binding energy and Fermi motion. Consider $f_N^A$, defined by

$$f_N^A(z)=\int d^3k\,\rho^A(\mathbf{k})\delta\left[z-\frac{k^+}{m_N}\right], \tag{2.2}$$

where $\rho(\mathbf{k})$ is the distribution of nucleon momenta $\mathbf{k}$ and $k^+=k^0+k^z$. For a free nucleon at rest, $k^0$ is just the nucleon mass $m_N$. For bound nucleons the shell model gives a good first approximation to the wave function. In that model the energy eigenvalue ($k^0$) of a nucleon in an orbital denoted by the quantum numbers $\alpha$ is simply $m_N-|\epsilon_\alpha|$, if the nucleon mass is included as part of the energy. Here we use $k^0\equiv m_N\eta\approx\langle m_N-|\epsilon_\alpha|\rangle$, in which the average is over occupied shell-model orbitals. Using the Fermi-gas distribution

$$\rho(\mathbf{k})=\frac{3}{4\pi k_F^3}\theta(k_F-|\mathbf{k}|),$$

one obtains[11]

$$f_N^A(z)=\frac{3}{4}\left[\frac{m_N}{k_F^A}\right]^3\left[\left[\frac{k_F^A}{m_N}\right]^2-(z-\eta)^2\right] \tag{2.3}$$

for $\eta-k_F/m_N\le z\le\eta+k_F/m_N$ and $f_N^A(z)=0$ otherwise. The smearing due to the distribution (2.3) enhances the valence distribution for small $x$, depletes it for medium $x$, and enhances it for $x\gtrsim 0.8$. Since $f_N^A(z)$ peaks at $z=\eta$, the basic effect of the factor $\eta$ is described by a rescaling $x\to x/\eta$ and this is responsible for most of the observed depletions at medium $x$ (Ref. 34).

Since the nucleons are bound by meson exchanges, one must include the mesons in the structure function. This is the role of the second pionic term of Eq. (2.1). [The influence of multipion exchanges is included by evaluating $f_\pi^A(y)$ using a correlated nuclear wave function.[12–15]] The pion cloud of a free nucleon contributes to DIS as in Fig. 2(a).

According to the parton model, the interaction with the virtual pion is an incoherent sum of contributions from the quarks and antiquarks in the pion. For this graph to contribute to DIS, the final-state nucleon must be on-shell: $(m_N-q^0)^2-\mathbf{q}^2=m_N{}^2$. This constraint is important: without it a further interaction between the nucleon and the pion debris would be needed to place the nucleon back on shell. Such processes are neglected here. Support for this comes from Llewellyn Smith's observation[35] that the pion debris is separated from the final-state nucleon by about 1.5 units of rapidity. Thus final-state interactions between the nucleon and the pion debris are suppressed.

The one-pion-exchange (OPE) process shown in Fig. 2(a) leads to a contribution

$$\delta^{\mathrm{OPE}}F_2^N(x,Q^2)=\int_x^1 dy\, f(y)F_2^\pi(x/y,Q^2)\ , \tag{2.4a}$$

to the intrinsic structure function of the nucleon, where

$$f(y)=\frac{3(g_{\pi NN})^2}{16\pi^2}y\int_{m_N{}^2y^2/(1-y)}^\infty dt\frac{t\,|F(t)|^2}{(t+m_\pi{}^2)^2}\ , \tag{2.4b}$$

is the distribution of virtual pions which contribute. In (2.4) $y$ is the fraction of the plus component of the nucleon carried by the pion, i.e., $p_\pi^+/p_N^+=(q^0+q^3)/m_N$. The $\pi NN$ coupling constant $g_{\pi NN}=13.5$; the invariant four-momentum squared of the pion is $-t$, and the elastic form factor at the $\pi NN$ vertex is $F(t)$. Ericson and Thomas relate $F(t)$ to $R$ the radius of a nucleon bag.[36]

For a nucleon in a nucleus, several standard nuclear-physics modifications should be made to the process in Fig. 2(a). First, the emission of low-momentum pions is Pauli-blocked by the nucleon Fermi sea. In addition, the pion may scatter off other nucleons in the nucleus before being struck by the photon. This scattering creates $NN^{-1}$ and $\Delta N^{-1}$ excitations of the nucleus [see Fig. 2(b)] and can be thought of as leading to an additional medium-dependent renormalization of the pion propagator. The production of $NN^{-1}$ and $\Delta N^{-1}$ excitations gives attraction. Were it not for the short-range repulsion, pion condensation would occur at ordinary nuclear matter densities. The needed short-range repulsion is conventionally parameterized as a contact interaction through the Landau-Migdal parameter $g'$ (Ref. 37) Ericson and Thomas use $g'=0.7$

All of these nuclear effects can be conveniently incorporated by the spin-isospin longitudinal response function per nucleon $R(\omega,|\mathbf{q}|)$. The response function is essentially the imaginary part of the pion's proper self-energy[14]

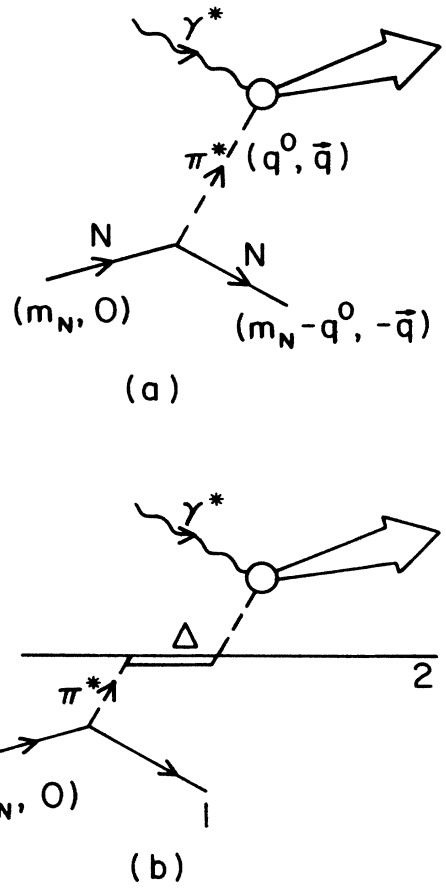


FIG. 2. Pion-cloud contribution to DIS: (a) free nucleon; (b) typical nuclear process.

that is caused by the scattering of the virtual pion by a nucleon. Taking the imaginary part guarantees that recoiling nucleons are on shell after the $\pi N$ scattering. See, for example, lines 1 and 2 in Fig. 2(b).

The integral over $t$ in (2.2) may be replaced by one over the $(\omega,|\mathbf{q}|)$ plane. Apart from smearing due to Fermi motion, the final-state nucleon must have excitation energy $\omega=\mathbf{q}^2/2m_N$, in the nonrelativistic approximation. The energy transfer must also satisfy the condition $\omega<|\mathbf{q}|-m_Ny$, which follows from $\mathbf{q}^2>q_3{}^2$ and the definition of $y$. Thus the distribution per nucleon of virtual pions contributing to DIS off a nucleus is[12]

$$\tilde{f}^A(y)=\frac{3g_{\pi NN}{}^2}{16\pi^2}y\int_{m_N{}^2y^2}^\infty d\mathbf{q}^2\int_0^{|\mathbf{q}|-m_Ny}d\omega\frac{\mathbf{q}^2|F(\mathbf{q}^2)|^2R(\omega,|\mathbf{q}|)}{(t+m_\pi{}^2)^2}\ , \tag{2.5}$$

where the replacement $t\to\mathbf{q}^2$ has been made in the numerator since $\omega\ll|\mathbf{q}|$.

The net result is an excess distribution of pions which contribute to the DIS process for a nucleon in a nucleus, over that for a free nucleon. This excess distribution is given by

$$f_\pi^A(y)=\tilde{f}^A(y)-f(y)\ . \tag{2.6}$$

This is shown in Fig. 3 for several values of the parameter $R$, with $k_F=1.30\ \mathrm{fm}^{-1}$, the value appropriate to Fe (Ref. 38). It is concentrated at quite low values of $y$, peaking at about $y=0.25$.

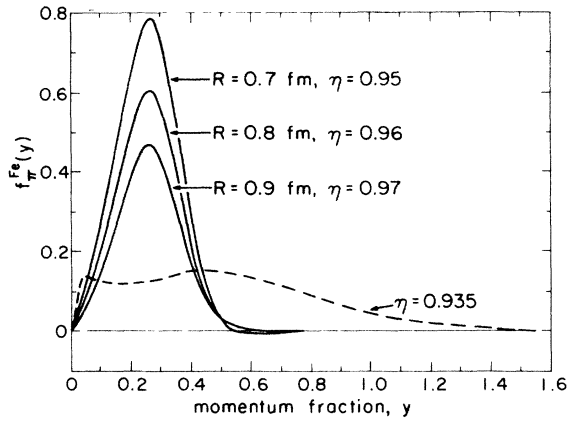


FIG. 3. The distribution of excess pions $f_\pi(y)$ for Fe in the Ericson-Thomas model (solid lines) and the model of Berger, Coester, and Wiringa (dashed line). The fraction of momentum carried by the nucleons is $\eta$.

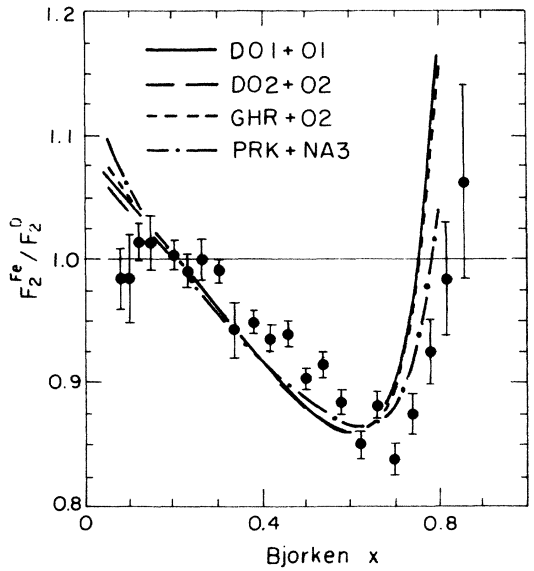


FIG. 4. The dependence on different nucleon and pion-quark distributions of the predicted ratio of Fe to D structure functions (Ref. 5) in the Ericson-Thomas pionic enhancement model (Refs. 14–16). The different curves all use $R=0.8$ fm, $k_F=1.30$ fm$^{-1}$, and $g'=0.7$.

Note that the above model treats nucleons and pions as elementary, except in their interactions with high-momentum virtual photons. This is really only appropriate for low momenta, or at large distances. Hence it only makes sense to use a pionic treatment of DIS at low $x$ (Refs. 35 and 39). Sizable pionic contributions at large $x$, if they had been obtained, would have been in a region where the model is not to be trusted.

For a model with nucleons and pions, the momentum-balance condition is that

$$1-\eta=\int_0^A dy\, y f_\pi^A(y)\ . \tag{2.7}$$

The shell-model binding energies are not known precisely and computations of $f_\pi^A(y)$ are model dependent. Here we compute $f_\pi^A(y)$ as shown below and obtain $\eta$ from the condition (2.7). This gives values very close to those obtained from tabulations of $\epsilon_\alpha$ (see Ref. 34).

The above prescriptions may be implemented within the framework of the parton model by defining the following medium-modified quark distributions:

$$q^A(x,Q^2)=\int_x^A \frac{dz}{z} f_N^A(z) q^N\left(\frac{x}{z},Q^2\right) + \int_x^A \frac{dy}{y} f_\pi^A(y) q^\pi\left(\frac{x}{y},Q^2\right)\ . \tag{2.8}$$

We need nucleon and pion distributions, so for the nucleon we use the two sets of Duke and Owens[40] (DO1 and DO2), those of Gluck, Hoffman, and Reya[41] (GHR), and the Big European Bubble Chamber (BEBC) parametrizations of Parker *et al.*[7,42] (PRK). For the pion we use the two sets of Owens[43] (O1 and O2) and the parametrization of the NA3 collaboration[44] (NA3). Figure 4 shows the results for the ratio of Fe to D structure functions. (The $Q^2$-dependent parametrizations are evaluated at 25 GeV$^2$.) For the $\pi NN$ form factor, we have used $R=0.8$ fm which Ericson and Thomas[12] now advocate.[13,14] A preferable value may even be closer to 0.9 fm (Refs. 2 and 36), and would give a smaller effect at all $x$. As can be seen, the pionic enhancement model gives a fair description of the data. The enhancement at low $x$ is due to the contribution of the excess pions to the nuclear ocean. The depletion at medium $x$ arises mainly from the imposition of momentum balance between the nucleons and excess pions while the rise at large $x$ is due to the Fermi motion of the nucleons.

As $Q^2$ increases, the effect is predicted to decrease slowly at both low and intermediate $x$. This is a result of the QCD scaling violations in the nucleon and pion structure functions.

The dependence of the EMC effect on the mass number $A$ can be accounted for in this model by varying the Fermi momentum $k_F$ (Refs. 34, 45, and 46).

There is an implementation of the pionic-enhancement model due to Berger, Coester, and Wiringa[15,47] which has several technical and philosophical differences from that of Ericson and Thomas. However, both versions use the convolution formula (2.1) and we may center our discussion on the differences in the functions $f_N^A(z)$ and $f_\pi^A(y)$. The nucleon distribution used by Berger, Coester, and Wiringa has a slightly narrower width than Llewellyn Smith's but the difference has no substantial effect. On the other hand, the excess-pion distributions, shown in Fig. 3, are very different since the distribution of Berger, Coester, and Wiringa extends to large $y$. This is disturbing because pions contribute to DIS at quite large $x$, where the pionic description is not appropriate. Since charged-lepton DIS includes a large valence-quark contribution at large $x$, it is not particularly sensitive to the shape of $f_\pi^A(y)$, and both treatments give similar descriptions of charged-lepton DIS. In other processes the long tail of $f_\pi^A(y)$ can give qualitatively different results, as we show in Secs. III–V.

The differences may be traced to the energy-conservation requirement. Berger, Coester, and Wiringa obtain their distribution by integrating out the transverse momenta from a pion density distribution $\rho(|\mathbf{q}|)$ calculated by Friman, Pandharipande, and Wiringa.[48] This density is simply a nuclear ground-state matrix element of the pion density operator, and so does not include the kinematic requirement of DIS, e.g., that the final-state nucleons for Fig. 2(b) be on shell. Final-state interactions between the nucleon emitting the pion and spectator nucleons could be invoked, but if the scattered nucleon is far off shell such final-state interactions are unlikely to be sufficient.

We conclude that the $f_\pi^A(y)$ calculated by Ericson and Thomas is a fair representation of the effects of pions on DIS off nuclei, while the distribution used by Berger, Coester, and Wiringa is not. However we use both models for purposes of illustration.

### B. Multiquark clusters

In multiquark cluster models[16–23] it is assumed that quark degrees of freedom play a role in nuclear wave functions at low momenta, through the formation of clusters in which six, nine, or more quarks are in close contact. Such clusters may form when two or more nucleons overlap appreciably. These objects can help explain a variety of nuclear phenomena,[49] but the evidence for their existence is ambiguous.

Neglecting the Fermi motion of both nucleons and clusters, the nuclear quark distributions in this approach are

$$q^A(x,Q^2)=(1-f_6^A)q^N(x,Q^2) + f_6^A(m_N/M_6)q^6(x,Q^2)\ . \tag{2.9}$$

Here $f_6^A$ is the fraction of nucleons in the nucleus $A$ which form six-quark clusters of mass $M_6$, while $q^6(x,Q^2)$ is the distribution per nucleon of quarks in those clusters. The additional factor $m_N/M_6$ arises because of the different masses of the clusters and a consequent difference in the natural scaling variables $z_n=(m_N/M_n)x$ for $n$-quark clusters. In practice one may take $M_n=(n/3)m_N$, and so $x$ has an expanded kinematic range.

Unfortunately, there is no experimental information on the quark distributions in multiquark clusters, $q^n(x,Q^2)$ for $n\geq 6$. These functions are determined from quark-counting rules,[50] combined with Regge expressions for the small-$x$ region. The resulting valence and ocean quark distributions have the forms

$$v^n(z_n)=\frac{3}{n}N_n(z_n)^{-1/2}(1-z_n)^{b_n}\ , \tag{2.10}$$

$$\bar{q}^n(z_n)=\frac{3}{n}\bar{N}_n(z_n)^{-1}(1-z_n)^{\bar{b}_n}\ . \tag{2.11}$$

The exponents $b_n$ are given in terms of the number of spectator quarks, $n_s$, by

$$b_n=2n_s-1+2|\Delta s_z|\ , \tag{2.12}$$

where $\Delta s_z=s_z(\text{target})-s_z(\text{quark})$. The distributions have been divided by $n/3$ so as to give the distribution per nucleon; the coefficients $N_n$ and $\bar{N}_n$ being those normalizations appropriate to the whole cluster. They are fixed by the requirement that there be $n$ valence quarks and by the condition that the sum of the momenta carried by quarks, antiquarks, and gluons is unity [or more precisely $(n/3)m_N/M_n$]. Only in the case of nucleons is there experimental information on the momentum fraction carried by gluons so the gluon momentum fraction is generally taken to be the asymptotic value expected from QCD (Ref. 51): $\langle x_g\rangle=8/(8+3N_f/2)$ where $N_f$ is the number of flavors of quarks.

This *ad hoc* use of counting rules has been criticized[35,39] because the $x$ region where data exist ($x\lesssim 0.7$) is nowhere near the edge of phase space ($x\simeq 2$). Indeed, even in the three-quark case formulas (2.10)—(2.12) only work qualitatively. The situation is likely to be worse for larger clusters. However, we believe that the underlying concept of a multiquark component in nuclear wave functions is a sensible one, and *there is one feature of these models which is insensitive to the detailed form of the quark distributions, namely, the expanded kinematic range in x which must extend at least to n/3.* This makes its presence felt in the distributions not just above $x=1$ but considerably below also.

The version of the multiquark cluster model which we employ is that of Carlson and Havens.[17] We now discuss how this model explains the DIS data. With (2.10) the six-quark cluster momentum distribution $zv^6(z)$, for $x=2z$ between 0.1 and 0.7, is depleted relative to the valence distribution $xv^3(x)$ in a nucleon. For $x\lesssim 0.1$, the ratio of the relative normalizations

$$\frac{1}{\sqrt{2}}N_6/(N_u+N_d)$$

may give an enhancement. Here $N_u$ and $N_d$ are the normalizations, as defined in (2.10), of $u$- and $d$-quark distributions in a nucleon and (for equal $u$ and $d$ distributions in the six-quark cluster) $N_6=N_6^u=N_6^d$ is three times the Carlson-Havens normalization. For $x\gtrsim 0.7$ the six-quark valence cluster distribution is enhanced because of the different kinematic range in $x$. Similarly, the large-$x$ ocean distribution in a cluster is also enhanced over that in a nucleon. At small $x$, the ocean may be enhanced or depleted, depending on a delicate balance between the relative normalizations and the exponents in the ocean distribution. Carlson and Havens use $\bar{N}_3=0.1857$ and $\bar{N}_6=0.5042$, the latter figure depending on both the assumed form of the valence distribution and the assumed fraction of momentum carried by the gluons. Their model has an ocean enhancement everywhere. Other reasonable nucleon distributions give a low-$x$ depletion for the same six-quark distributions.

In Fig. 5 we show the predictions of the Carlson-Havens model for the ratio of structure functions $F_2$ in Fe and D. In addition to the same four sets of nucleon distributions used in Fig. 4 for the pion model we have used the counting-rule distributions of Carlson and Havens (CH). The model is very sensitive to the details of the six-quark cluster and nucleon distributions. This indicates that cluster models are poorly defined.

Carlson and Havens chose $f_6=0.3$, which fits the EMC

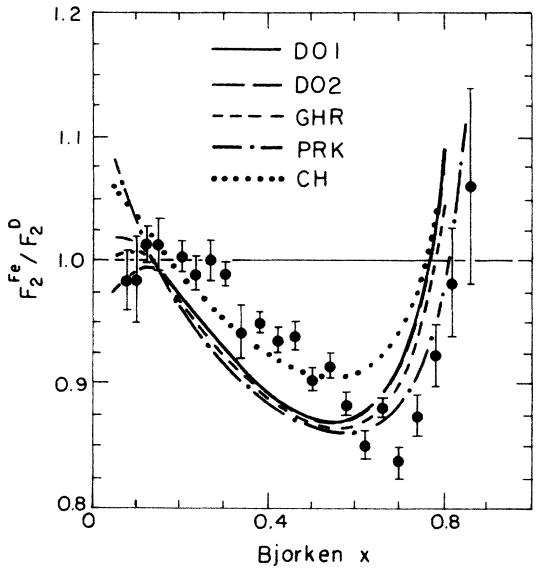


FIG. 5. Carlson-Havens six-quark cluster model (Ref. 17) for the ratio of structure functions for Fe to D, using different nucleon structure functions but fixed six-quark structure function. The six-quark probability is taken to be $f_6=0.3$.

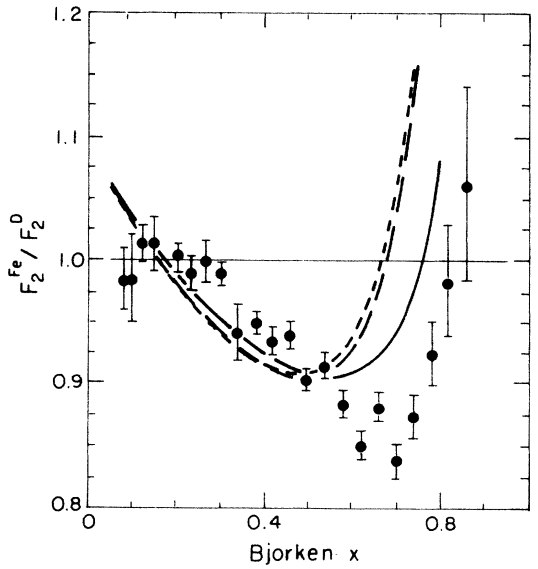


FIG. 6. Fermi motion in the Carlson-Havens model. Solid curve: original model of Carlson and Havens. Long-dashed curve: nucleon Fermi momentum $k_F=1.30$ fm$^{-1}$. The short-dashed curve also includes Fermi motion of the six-quark clusters.

data. This may seem a little large. However there are a lot of pairs of nucleons in a nucleus and the probability per pair of forming a six-quark cluster is actually quite small. Pirner and Vary[18] have estimated that $f_6$ is about 0.2 in Fe, which is in accordance with the calculations of Greben and Thomas.[52] Given the uncertainties in the model, we continue to use the Carlson and Havens value. The $A$ dependence of the model is incorporated by allowing $f_6$ to vary roughly as the nuclear density.[18]

Carlson and Havens did not include "Fermi motion" for either nucleons or clusters. However, this motion is a consequence of the medium- and long-range interactions between nucleons, while formation of multiquark clusters, if it occurs, is a property of the short-distance $NN$ wave function. Hence it is appropriate to include at least the Fermi motion of the nucleons.[18] We have done so by simply convoluting the nucleon distributions in Eq. (2.9) with a Fermi distribution (2.7). We have also included motion of the six-quark clusters, assuming that the total momentum of a cluster is just the sum of the momenta of the nucleons which formed it, but this is a small effect. The results are shown in Fig. 6. The Fermi motion of the nucleons leads to a rise in the ratio at considerably smaller values of $x$ than in the data. This seriously undermines the ability of this particular model to reproduce the DIS data. Nevertheless, it does not weaken the more general feature that an increased kinematic range in $x$ produces characteristic signatures at medium $x$.

### C. Rescaling

The third approach is a rescaling of the momentum-transfer dependence of parton distributions. All models in this class stem from the original observation by Close, Roberts, and Ross[24] that, at least over the limited range $0.2 \lesssim x \lesssim 0.7$, the structure function of a heavy nucleus measured at a scale $Q^2$ is similar to that of an isolated nucleon at a higher scale $\xi_{NA}Q^2$:

$$F_2^A(x,Q^2)=F_2^N(x,\xi_{NA}Q^2) . \tag{2.13}$$

These authors term this effect "dynamical rescaling." They interpret it as being due to a change in a fundamental length scale—presumed to be the confinement size—of a nucleon, when that nucleon is immersed in a nuclear environment. See also Ref. 53.

The observation that the EMC data can be described by (2.13) is a phenomenological fact. It is not, in itself, a model for the EMC effect. Some specific dynamics must be employed to compute $\xi_{NA}(Q^2)$ for a single $A$ at a given $Q^2$, and this leads to uncertainty.

If dynamical rescaling holds, the quantum chromodynamics (QCD) has some immediate implications. Consider[24] the moments of the structure function per nucleon:

$$M_n^A(Q_A{}^2)=\int_0^A dx\, x^{n-2}F_2^A(x,Q^2) . \tag{2.14}$$

The observation of Close, Roberts, and Ross implies

$$M_n^A(Q_A{}^2)=M_n^N(\xi_{NA}Q_A{}^2) . \tag{2.15}$$

The interesting feature is that $\xi$ is roughly independent of $n$. In leading order the QCD renormalization group predicts the $Q^2$ evolution of flavor-nonsinglet moments to be

$$M_n^A(Q_A{}^2)=\left[\frac{\alpha_s(Q_A{}^2)}{\alpha_s(\mu_A{}^2)}\right]^{d_n^{\rm NS}} M_n^A(\mu_A{}^2) , \tag{2.16}$$

where $d_n^{\rm NS}$ is a calculable coefficient. It follows that $\xi$ must increase with $Q^2$. Using the renormalization-group equation for the QCD coupling constant,

$$\alpha_s^{-1}(\xi Q^2)=\frac{\beta_0}{4\pi}\ln\xi+\alpha_s^{-1}(Q^2)\ , \tag{2.17}$$

one finds that

$$\xi_{NA}(Q_A^2)=[\xi_{NA}(\mu_A^2)]^{\alpha_s(\mu_A^2)/\alpha_s(Q_A^2)}\ . \tag{2.18}$$

This is independent of $n$ and hence preserves the independence of $\xi(\mu^2)$. Higher-order corrections to (2.18) do generate a specific $n$ dependence so the $x$ independence of $\xi$ cannot be exact. However, the second-order corrections to (2.16) are not very large for $n=3$—8 and an approximate $x$ independence in the range $0.2\lesssim x\lesssim 0.8$ can be maintained.[25,26]

It is natural to interpret dynamical rescaling as originating in some dynamics at low $Q^2$, appropriate to the confinement regime of QCD. Various dynamical models for this low-$Q^2$ effect have been proposed[54–57] in addition to that of Jaffe *et al.*[25] Whichever of these models proves valid, the concept of dynamical rescaling affords a useful model-independent way of parametrizing data and this alone we now pursue.

Close *et al.*[24–26] implement dynamical rescaling by making a fit to the EMC data on deuterium, and evolving this fit with second-order Altarelli-Parisi[58] equations using four flavors and $\Lambda_{\overline{\rm MS}}=250$ MeV ($\overline{\rm MS}$ denotes the modified minimal-subtraction scheme). We shall, for simplicity, merely employ the $Q^2$-dependent distributions[40,41] used earlier. However, this is not without its problems. All of these distributions have been obtained by taking fits to the data at $Q_0^2=4$ GeV$^2$, evolving with first-order Altarelli-Parisi equations and then parametrizing the results. But this involves $\Lambda_{\rm LO}$ (LO denotes leading order), which cannot be extracted unambiguously from the data.[59] Despite the ambiguities, the parametrizations that we use yield a $Q^2$ dependence of $\alpha_s$ that is consistent with various data.[40,41,60]

This brings us to a short discussion of the values of $\Lambda_{\rm LO}$ used. The two sets of nucleon distributions given by Duke and Owens[40] and the pion distributions given by Owens[43] correspond to different gluon distributions: DO1 and O1 have a soft distribution and $\Lambda_{\rm LO}=200$ MeV (which corresponds roughly to $\Lambda_{\overline{\rm MS}}=250$ MeV) while DO2 and O2 have a hard distribution and $\Lambda_{\rm LO}=400$ MeV. Gluck, Hoffman, and Reya[41] also have a hard gluon distribution and $\Lambda_{\rm LO}=400$ MeV. This is not equivalent to the value of $\Lambda_{\rm LO}$ in the DO2 and O2 distributions because Duke and Owens evolve with four flavors while Gluck, Hoffman, and Reya evolve with only three.

Thus dynamical rescaling corresponds to using the medium-modified quark distributions

$$q^A(x,Q_A^2)=q^N(x,\xi_{NA}Q_A^2)\ , \tag{2.19}$$

where $\xi_{NA}(Q_A^2)$ is given by (2.18). To implement this equation we use the values for $\xi_{NA}(\mu_A^2)$ given in Table II of Close *et al.*[26] for $\mu_A^2=20$ GeV$^2$. These values provide a good fit[26] to the available charged-lepton DIS data, so the details of the model of Close *et al.* are irrelevant. Strictly, we should refit $\xi$ for each distribution but we find this to be unnecessary. We note that by using a value such as 20 GeV$^2$ as a reference point, the effects of uncertainties in $\Lambda_{\rm LO}$ are minimized. This is in contrast with using a small value of the order of 0.5 GeV$^2$, as in Refs. 25 and 26, for which these uncertainties exacerbate the problems associated with using perturbative QCD in such a low-momentum region.

The effects of QCD rescaling on the quark distributions cause a shift of the momentum from the medium- and high-$x$ regions to lower $x$ values. Thus the dynamical rescaling model predicts characteristic enhancements at low $x$ and depletions at medium $x$ in both the valence- and ocean-quark distributions.

The predicted results for charged-lepton DIS are shown in Fig. 7. Although the model is unreliable outside the region $0.2\lesssim x\lesssim 0.8$, because of the higher-order distortions discussed above, we extrapolate the results outside this region in the hope that this will not be misleading. All three distributions provide a fair fit to the data although they do not agree as well as the results given by Close, Jaffe, Roberts, and Ross[26] (CJRR). In particular, the point at which the ratio passes through unity occurs here at a smaller value of $x$. This has also been noticed by Berger and Coester[47] who, in addition to using the DO1 distributions, also made a fit to the EMC Fe data and rescaled that by $1/\xi$. Small changes with $Q^2$ are not sufficient to explain the difference. We therefore attribute it to a rather different $D$ structure function used by Close, Roberts, and Ross[24] (CRR), which they obtained by a QCD fit to the EMC D data. In particular, the CRR parametrization of $F_2(x,Q^2)$ has a significant rise with $Q^2$ at $x=0.125$ and is approximately independent of $Q^2$ at $x=0.175$. Thus the CJRR ratio of Fe to D structure functions is unity at $x\approx 0.2$. However, all of the other structure functions are approximately independent of $Q^2$ at $x\approx 0.1$. A close look at the EMC D data (Fig. 1, Ref. 61) shows that $F_2(x,Q^2)$ is nearly constant ($=0.3$) at $x\approx 0.125$.

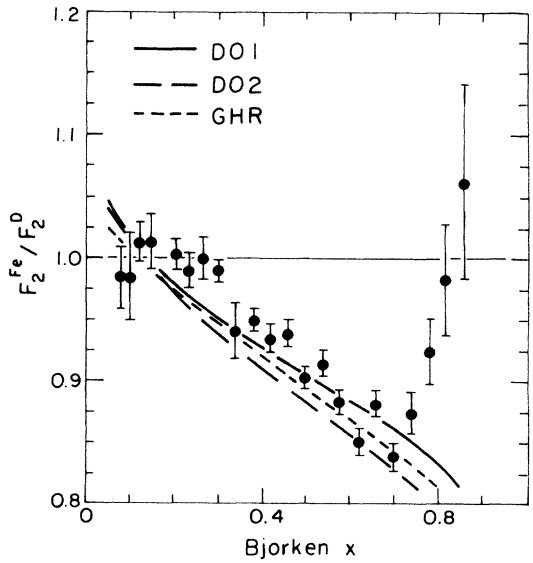


FIG. 7. Dynamical rescaling model of the ratio of structure functions for Fe to D (Ref. 5), for different nucleon structure functions. $Q_{\rm Fe}^2$ is taken to be 25 GeV$^2$.

Nonetheless, it is worth noting that the value of $x$ at which the ratio passes through unity is a characteristic prediction of dynamical rescaling; there is no possibility of obtaining a ratio differing from unity in this region. Hence it would be of interest to better determine this $x$ value.

The low-$x$ enhancement in this model diminishes in size as $Q^2$ increases because the ocean quark distributions evolve logarithmically. While $\xi_{NA}(Q_A{}^2)$ is increasing, the ratio of distributions is not. The medium-$x$ depletion remains essentially constant in the presently accessible range of $Q^2$.

One striking aspect of Fig. 7 is the absence of a rise in the ratio at large $x$. This deficiency is due to the neglect of Fermi motion. In order to incorporate it one needs a detailed model of the dynamical origins of $\xi$. We have tried using a naive Fermi smearing

$$q^A(x,Q_A{}^2)=\int_x^A dz\, f_N^A(z) q^N(x,\xi_{NA}Q_A{}^2)\ , \tag{2.19}$$

but, this leads to an overcorrection and severe disagreement with data for $x>0.6$. Nevertheless, while the incorporation of Fermi motion is a problem which must be addressed by models in this class, we have no reason to believe that the deficiency cannot be rectified. The predicted depletion is the region $x\gtrsim 0.7$ is therefore dismissed as an artifact. We do regard the medium-$x$ depletion and the low-$x$ enhancement as a characteristic and testable feature.

## III. NEUTRINOS

Neutrino DIS affords the possibility of extracting separate valence and ocean distributions because neutrino- and antineutrino-induced weak interactions are different and because parity violation admits the presence of an additional term.

Several sets of data are now available on the nuclear dependence of DIS of neutrinos and antineutrinos. The BEBC—track-sensitive target (TST) (WA24) collaboration[7] have compared $\nu$ and $\bar{\nu}$ charged-current cross sections and structure functions for Ne and $H_2$ targets. No nuclear dependence was found in the region $0.0<x<0.65$ and $1.2<Q^2<20$ GeV$^2$, but the statistical errors were large. An IHEP-ITEP Soviet collaboration[8] have reanalyzed their $\bar{\nu}$ data on a Ne-$H_2$ target in the 15-ft bubble chamber at Fermilab and compared with $\bar{\nu}$ data on D obtained with BEBC at CERN. A definite nuclear effect was observed in the differential cross section $d\sigma/dx$, including an enhancement around $x=0.2$ and a large depletion for $x=0.6$–$0.7$. The WA25 and WA59 collaborations have compared[9] their respective BEBC data on D and Ne-$H_2$ targets, obtained with the same wide-band $\bar{\nu}$ beam. In addition to data on $d\sigma/dx$ they have presented data on $d\sigma/dy$ and investigated the $Q^2$ dependence over the range $0.25<Q^2<26$ GeV$^2$. Their data are compatible with the charged-lepton data in the range $0.3<x<0.6$ but they found no low-$x$ rise in the ratio $(d\sigma^{\rm Ne}/dx)/(d\sigma^{\rm D}/dx)$, for isoscalar Ne and D, independent of $Q^2$ (up to $Q^2\sim 14$ GeV$^2$). The CERN-Dortmund-Heidelberg-Saclay (CDHS) (WA1) collaboration[10] has compared $\nu$ and $\bar{\nu}$ data for Fe and $H_2$ targets in the range $3<Q^2<40$ GeV$^2$. They present data on the ratio $F_2^{\rm Fe}/F_2^{\rm H_2}$ and the ratio of ocean quark distributions. In neither case was a significant deviation from unity observed but the statistical errors are large.

The predictions for the neutrino and antineutrino structure functions and cross sections of the three models discussed in the preceding section may be calculated by using the appropriate medium-modified quark distributions: Eqs. (2.8), (2.9), and (2.19). Inserting these into standard expressions for neutrino structure functions shows that the resulting nuclear structure functions are obtained in terms of the nucleon, pion, and six-quark structure functions. Thus, for example, in the pionic enhancement model one obtains convolutions on $F_2$ and $xF_3$ which are analogous to Eq. (2.5). For pions, we have the structure functions

$$F_2^{\nu\pi}(w)=2w[v_\pi(w)+d_0(w)+s_0(w)+\bar{u}_0(w)+\bar{c}_0(w)] \tag{3.1}$$

and

$$F_3^{\nu\pi}(w)=2[s_0(w)-\bar{c}_0(w)]\ , \tag{3.2}$$

where $w$ is the momentum fraction of a quark in the pion. We assume isospin symmetry and average over $\pi^+$ and $\pi^-$. For six-quark bags one similarly finds, for the structure functions per nucleon:

$$F_2^{\nu q^6}(z_6)=2z_6[d_v^6(z_6)+d_0^6(z_6)+s_0^6(z_6)+\bar{u}_0^6(z_6)+\bar{c}_0^6(z_6)]\ , \tag{3.3}$$

$$F_3^{\nu q^6}(z_6)=2[d_v^6(z_6)+s_0^6(z_6)-\bar{c}_0^6(z_6)]\ , \tag{3.4}$$

$$F_3^{\bar{\nu}q^6}(z_6)=2[u_v^6(z_6)-\bar{s}_0^6(z_6)+c_0^6(z_6)]\ , \tag{3.5}$$

where we have assumed isospin symmetry in the six-quark ocean. The charmed ocean in a six-quark bag is neglected. (Note that the valence and ocean distributions used here are defined per nucleon so $2d_v^6$ and $2u_v^6$ are each three times the valence distribution of Carlson and Havens.)

In Fig. 8 we show the CDHS data[10] for $F_2^{\rm Fe}/F_2^{\rm H_2}$ and the predictions of the three models using the same nucleon distributions. The mean $Q^2$ of the CDHS data varies approximately as $66x$ GeV$^2$. We have evaluated the momentum-dependent distributions at a constant 4 GeV$^2$, the lowest at which they are valid, because this corresponds to the mean $Q^2$ of the low-$x$ data and because the models do not predict any strong $Q^2$ dependence in this ratio at medium $x$. Any discrepancy with the lowest-$x$ data point (for which $\langle Q^2\rangle=3$ GeV$^2$) could be attributed either to shadowing or to the value of $Q^2$ being so low that the parton model is invalid. The rest of the data is entirely consistent with each of the model predictions. The data is also consistent with no nuclear effect.[10]

Neutrino and antineutrino double-differential cross sections may be integrated to obtain $d\sigma/dx$ and $d\sigma/dy$. The predictions for $(d\sigma^{\bar{\nu}{\rm Ne}}/dx)/(d\sigma^{\bar{\nu}{\rm D}}/dx)$ are shown in Fig. 9, along with the WA25/WA59 $\bar{\nu}$ data.[9] (For Ne we have used $k_F^{\rm Ne}=1.15$ fm$^{-1}$ and $f_6^{\rm NE}=0.25$.) The predicted curves closely resemble those for the ratios of $F_2$ (in both the weak and electromagnetic cases), with nuclear effects

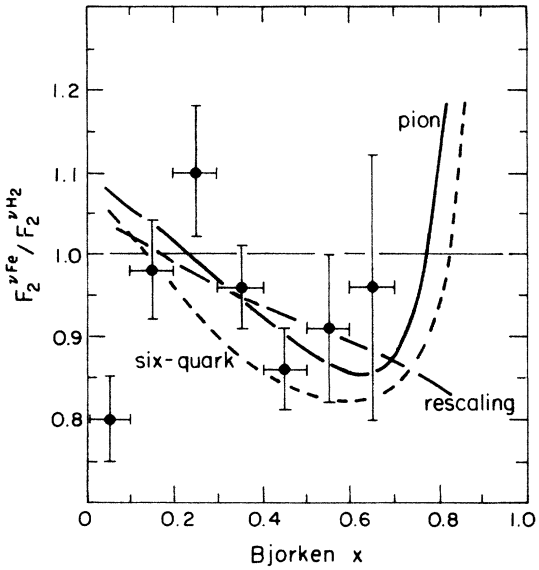


FIG. 8. The CDHS data on the ratio of the neutrino structure functions $F_2$ for Fe to $H_2$. Pion model (Ref. 12) (solid curve), the six-quark model (short-dashed curve), and the dynamical rescaling model (long-dashed curve). All models here utilize the DO1 distributions for D. The pion structure function is based on the O1 distributions and the six-quark structure function is based on the CH distributions. The momentum-dependent distributions are all evaluated at fixed $Q^2=4$ GeV$^2$.

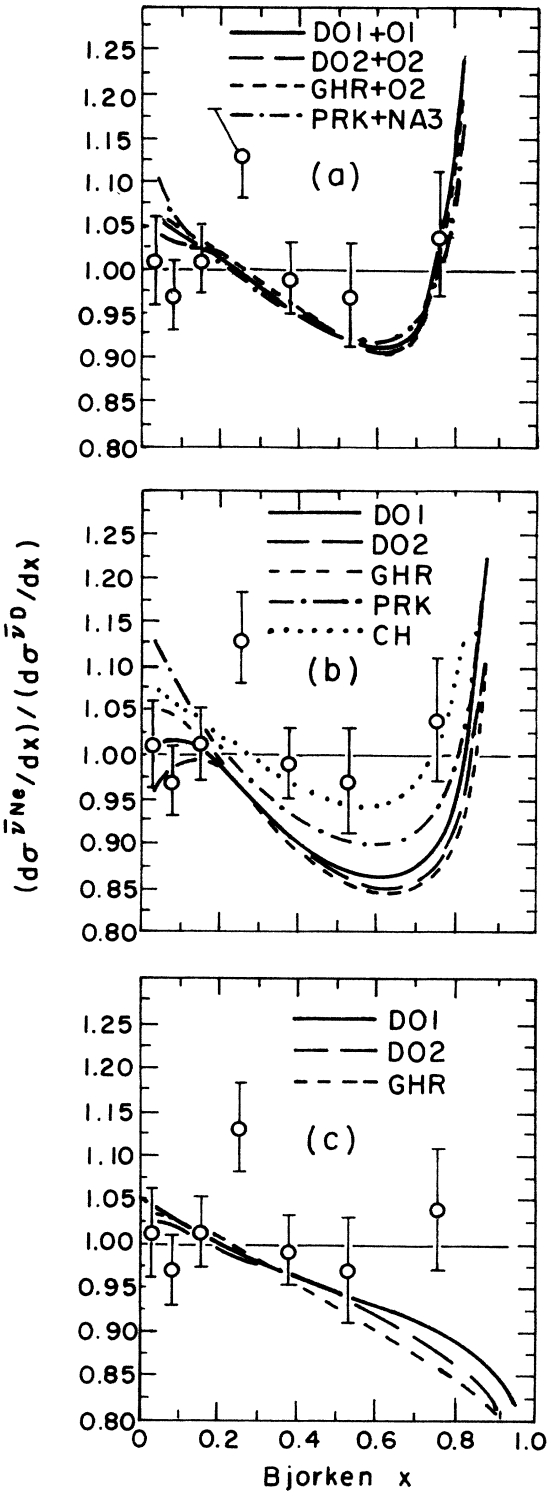


FIG. 9. The WA25/WA59 data on the ratio of the differential cross section $d\sigma^{\bar{\nu}}/dx$ for Ne to D. Model predictions: (a) pion model (Ref. 12); (b) six-quark model; (c) dynamical rescaling.

generally being a little smaller than for Fe. Therefore this ratio does not provide new information.

In contrast, the $d\sigma/dy$ $\bar{\nu}$ and $\nu$ data *do* contain information not accessible to electron or muon scattering. Predictions of the various models are shown in Fig. 10 together with the $\bar{\nu}$ data from Ref. 9 and preliminary $\nu$ data from the same experiment. As can be seen there are no dramatic effects. However, a comparison between the $\bar{\nu}$ and $\nu$ cross sections places new constraints on the models. None of the models provides an excellent fit but once again the errors are large and it is doubtful that the small apparent discrepancies are significant. Because of the dependence on the distributions used, all models must be judged in agreement with the data (cf. Ref. 9). In the case of the six-quark model the distributions which fit the $\bar{\nu}$ data best do worst on the $\nu$ data and vice versa. Nevertheless, given the preliminary nature of the $\nu$ data, and the large errors, the model cannot be ruled out.

The double-differential cross section for $\bar{\nu}$ scattering at large $y$ is a direct measure of the antiquark distribution in the target.[10] Specifically,

$$\frac{d^2\sigma^{\bar{\nu}A}/dx\,dy\,|_{y=1}}{d^2\sigma^{\bar{\nu}p}/dx\,dy\,|_{y=1}}=\frac{x\{[\bar{u}(x)+\bar{d}(x)]/2+\bar{s}(x)\}^A}{x[\bar{d}(x)+\bar{s}(x)]^p}\,. \tag{3.6}$$

Unfortunately, $y=1$ is difficult to obtain experimentally and a fit must be used to extract the antiquark distribution. This process introduces very large errors and no $p$ data is available for $x>0.25$. The CDHS data for small $x$ and the predictions of the various models are shown in Fig. 11. All three models agree within the large errors. Interestingly, there are tantalizing qualitative differences between these models in the experimentally unmeasured

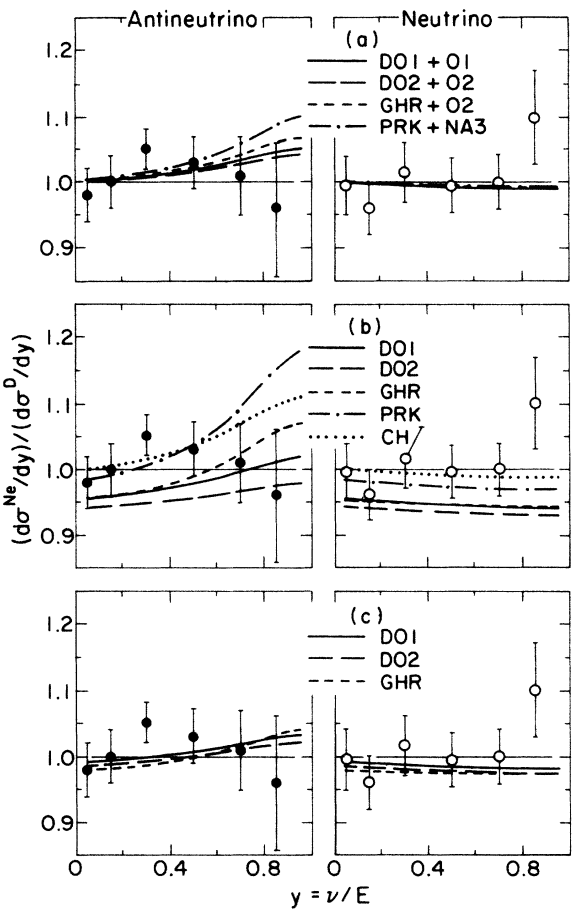


FIG. 10. The WA25/WA59 data on the ratio of $d\sigma^{\bar{\nu}}/dy$ for Ne to D compared with preliminary data from the same experiment on the corresponding ratio for neutrinos. Model predictions: (a) pion model (Ref. 12); (b) six-quark model; (c) dynamical rescaling.

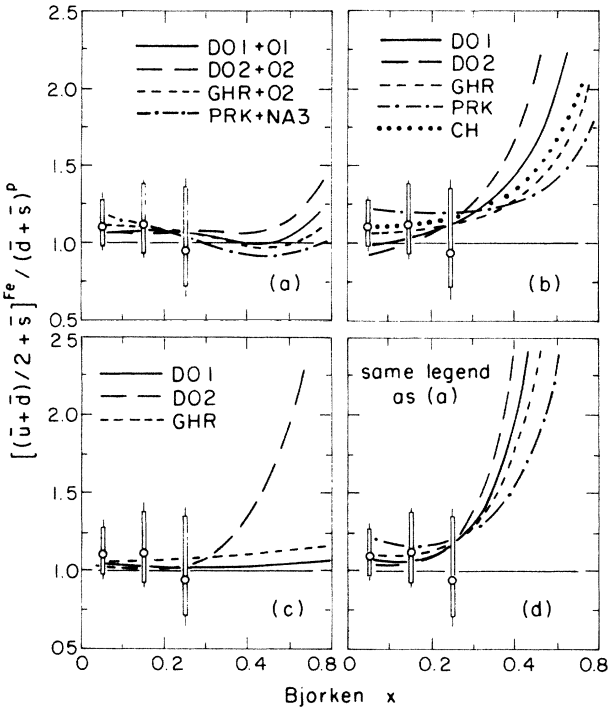


FIG. 11. The CDHS data on the ratio of the ocean-quark distributions in Fe to those in D. Model predictions: (a) Ericson-Thomas pion model; (b) Carlson-Havens six-quark model; (c) dynamical rescaling; (d) pion model of Berger, Coester, and Wiringa.

region. Unfortunately the experimental situation looks hopeless.

In connection with the predicted behavior of the tail of the ocean distributions we would like to draw attention to the very sharp rise in the ratio that occurs in the version of Berger, Coester, and Wiringa of the pion model. The predictions are shown in Fig. 11 for comparison, with the same Fermi distribution as in the Ericson and Thomas version. The predicted cross section only falls by about 2 orders of magnitude at $x=1$ from its value at $x=0.25$ while in all the other models it essentially vanishes. This is due to the contribution from the valence antiquark in the pion, which in the model of Berger, Coester, and Wiringa can carry a sizable fraction of the momentum of the nucleus. Not surprisingly, the predictions of Berger, Coester, and Wiringa for the ocean which agree poorly with antineutrino[10,62] data on heavy nuclei [see Fig. 17(b) of Ref. 10 and Table 5 of Ref. 62] are in disagreement with antiquark distributions obtained from existing Drell-Yan data.[63,64] See below.

The ratio (3.6) may be integrated over $x$ to obtain

$$R^{A}_{\mathrm{CDHS}}=\frac{d\sigma^{\bar{\nu}A}/dy\,|_{y=1}}{d\sigma^{\bar{\nu}p}/dy\,|_{y=1}} \tag{3.7}$$

which is the $y=1$ limit of the ratio in Fig. 10. The experimental value for Fe is[10] $R^{\mathrm{Fe}}_{\mathrm{CDHS}}=1.10\pm0.11\pm0.07$. Contrary to the claims of Abramowicz *et al.*[10] a larger value is not implied by the EMC muon data. For the various distributions used in Fig. 11, the predictions of the pion model[65] are in the range $1.07\leq R^{\mathrm{Fe}}_{\mathrm{CDHS}}\leq 1.16$, those of the six-quark model are in the range $0.98\leq R^{\mathrm{Fe}}_{\mathrm{CDHS}}\leq 1.22$, and those of the rescaling model are in the range $1.04\leq R^{\mathrm{Fe}}_{\mathrm{CDHS}}\leq 1.06$.

## IV. NUCLEAR $J/\psi$ PRODUCTION

The EMC effect shows that the quark distribution functions per nucleon are not the same as for free nucleons. Determining the precise nature of the changes is a subject of high interest so one should also ask if the nucleus modifies gluon distribution functions. Apart from the overall fraction of momentum carried by the gluons, DIS tells us nothing about the gluon distributions, so information on the gluons is a potential means of discriminating models.

Finding accurate probes of gluons in the nucleus (or even for the nucleon) is very difficult. Lepto-, photo-, and hadroproduction of heavy mesons ($J/\psi$ or $\Upsilon$), as well as direct production of high-$p_T$ photons, are all sensitive to the gluon distributions in nuclear targets. However, heavy

meson production suffers from theoretical uncertainties in the reaction mechanism, while direct photon production requires colliding beam experiments. To date, only electromagnetic $J/\psi$ production has been suggested as a means to compare gluon distributions in heavy and light targets.[66]

In lowest-order QCD, the mechanism for electromagnetic production of a heavy quark-antiquark pair is the fusion of a real or virtual photon with a target gluon. This photon-gluon fusion model,[67] usually used in analyzing $J/\psi$ production, accounts reasonably well for the experimental data.[68] In the model, the cross sections for both quasielastic (where the photon energy is close to that of the $J/\psi$) and inelastic production are proportional to the gluon distribution function of the target.[67] Thus one can hope that the comparison of $J/\psi$ production from heavy nuclei with that from hydrogen or deuterium can provide useful information about the nuclear gluon distributions. However, the neglect of final-state interactions (which depend on $A$) involved in the formation of the bound meson state may not be justified.[69,70]

The ratio of the total cross sections for inclusive $J/\psi$ production on iron and $H_2$/D is plotted against $M_\psi{}^2/2m_N\nu$ in Fig. 12. (Here $\nu$ is the energy carried by the photon.) In the photon-gluon fusion model, this ratio is equal to the ratio of the gluon distribution functions in iron and an isolated nucleon, and the quantity $M_\psi{}^2/2m_N\nu$ is essentially the momentum fraction $x$. Note that data exist only for very small values of $x$ ($<0.08$). Averaging the experimental ratios of Fig. 12 over the available region of $x$ one finds that[30]

$$\sigma^{\mathrm{Fe}}/\sigma^{\mathrm{D}}=1.45\pm0.12\ \text{(statistical)}$$
$$\pm0.22\ \text{(systematic)}\ . \tag{4.1}$$

We now confront the various models for the EMC effect with this $J/\psi$ data. Since gluons are found in pions as well as nucleons, pion enhancement models predict a nuclear modification of the gluon distribution per nucleon. Rough estimates of the gluon distributions can be obtained from counting rules. These give

$$xg^N(x)=6\langle x_g\rangle_N(1-x)^5 \tag{4.2}$$

for the nucleon, but

$$wg^\pi(w)=4\langle w_g\rangle_\pi(1-w)^3 \tag{4.3}$$

for the pion; where $\langle x_g\rangle$ and $\langle w_g\rangle$ are the momentum fractions carried by the gluons. Typically $\langle x_g\rangle$ and $\langle w_g\rangle$ are about $\frac{1}{2}$. Estimates of $g^\pi(w)$ from $J/\psi$ production[71] suggest a somewhat smaller exponent of $1-w$ than that in (4.3). Hence we have also investigated

$$wg^\pi(w)=3\langle w_g\rangle_\pi(1-w)^2\ . \tag{4.4}$$

The nuclear-gluon-distribution function in the pion enhancement model is [cf. Eqs. (2.1) and (2.8)]

$$xg^A(x)=\int_x^A dz\, f_N^A(z)\frac{x}{z}g^N\left[\frac{x}{z}\right]+\int_x^A dy\, f_\pi^A(y)\frac{x}{y}g^\pi\left[\frac{x}{y}\right]. \tag{4.5}$$

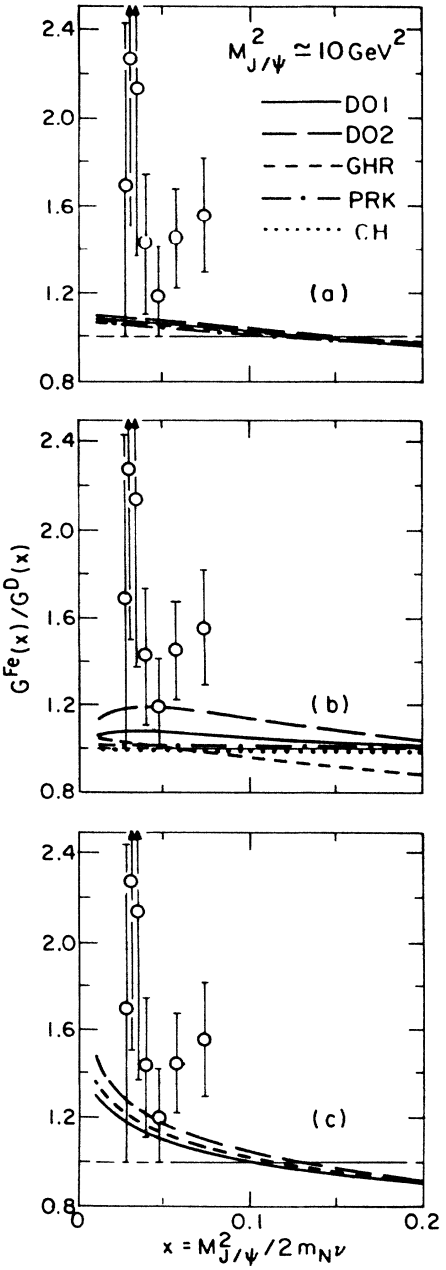


FIG. 12. Ratios of inclusive muoproduction $J/\psi$ cross sections (Ref. 30) vs $x=M_{J/\psi}{}^2/2m_N\nu$ for different nucleon distribution functions: (a) pion enhancement; (b) six-quark cluster; (c) dynamical rescaling.

As in the comparison with DIS we use the nucleon momentum distribution of Eq. (2.3), derived from the Fermi gas model. Since $x$ is very small, the function $(x/y)g^\pi(x/y)$ may be replaced by its value at $x=0$. The remaining integral on $y$ is strongly constrained by the DIS data. Thus the approaches of Ericson and Thomas and Berger, Coester, and Wiringa yield very similar results here. For the gluon distribution in the pion we use the parametrizations of Owens[43] in connection with the

momentum-dependent nucleon gluon distributions of Duke and Owens[40] and Gluck, Hoffman, and Reya[41] while we use Eq. (4.4) with $\langle w_g \rangle_\pi = 0.47$, appropriate to the NA3 distributions, in conjunction with Eq. (4.2) and $\langle x_g \rangle_N = 0.54$, which is appropriate to the distributions of Parker *et al.*[7] The computed ratios of gluon distribution functions are shown in Fig. 12(a) and fall somewhat below the data. There is little dependence on the parametrization used for the nucleon and pion gluon distributions. It would appear to be difficult for this model to increase the ratio substantially because it is constrained by the number of excess pions per nucleon which is necessarily quite small (about 0.14).

For the six-quark cluster model we have assumed, in the spirit of Carlson and Havens, that the gluon distribution per nucleon in the six-quark cluster is given by

$$z_6 g^6(z_6) = (12\langle z_g \rangle_6/2)(1-z_6)^{11} . \tag{4.6}$$

Because of the assumption by Carlson and Havens that the momentum fraction, $\langle z_g \rangle = 0.57$, carried by gluons in a six-quark cluster is the same as for a nucleon, this once more leads to ratios quite close to unity, as shown in Fig. 12(b). Note that there is little reason for assuming an equality between $\langle x_g \rangle_N$ and $\langle z_g \rangle_6$, but finding a justification for invoking a difference would be difficult.

According to the intuitive arguments of Refs. 24 and 26 concerning the origin of dynamical rescaling in an increased confinement size, it is natural to expect that a nuclear gluon distribution will be related to that in a nucleon by[72]

$$g^A(x,Q_A^2) = g^N(x,\xi_{NA} Q_A^2) . \tag{4.7}$$

Such a relation must hold if rescaling is to apply to the singlet quark distribution, since the evolution equations couple it and the gluon distribution. The resulting ratio of iron to "nucleon" gluon distributions is shown in Fig. 12(c). We have used $\xi_{NA} = 1.87$ and 1.83 for $\Lambda_{\rm LO} = 200$ and 400 MeV, respectively, according as to which of three different parametrizations of the nucleon-gluon-distribution function is employed. All sets lead to ratios somewhat smaller than the observations. Although DO1 is a "soft"-gluon distribution, while DO2 and GHR are "hard," the major difference in the ratios is due to the use of three light flavors by GHR and their associated treatment of thresholds, whereas DO use four flavors. The differences shown in Fig. 12(c) reflect mainly the uncertainties in current knowledge of the gluon distribution in a nucleon. Furthermore,[72] "dynamical rescaling is strictly only well founded for $0.2 < x$." Thus the use of the $x$-independent predictions for $\xi_{NA}$ at $Q_g^2 = M_{J/\psi}^2$ is not justifiable within the terms of the model.

The problem of nuclear contamination in the distributions is an important worry. Almost all information on the gluon distribution has been obtained from nuclear data. The DO1 distribution is directly constrained by $J/\psi$ production on a variety of nuclear targets and indirectly by high-mass (Drell-Yan) dimuon production in both $p$ nucleus and $pp$ collisions. DO2 and GHR are determined from scaling violations $\partial F_2(x,Q^2)/\partial \ln(Q^2)$, but DO2 is also constrained by $pp$ Drell-Yan data. Of the three, nuclear contamination is expected to be the most problematic for DO1. In the pion and rescaling models most contamination is expected to cancel in the ratio. This may be explicitly checked in the case of dynamical rescaling by assuming that the three distributions are exactly those appropriate to Fe. We find that this assumption does lead to an appreciable increase in the ratios at low $x$ but that increase is still less than the difference between the three distributions shown in Fig. 12(c). Given also that we have made no attempt to accurately fit the parameter $\xi$ in the case $\Lambda_{\rm LO} = 400$ MeV, we conclude that the curves in Fig. 12 are not misleading.

Although the $J/\psi$ data suggest a substantial enhancement in the nuclear gluon distribution, they are available only at very small values of $x$, where all of the models have great uncertainties. There are also problems associated with the photon-gluon fusion model. The rescaling model can predict a significant nuclear enhancement of $g^A(x)$, but this depends on the choice of nucleon gluon distribution. Nuclear $J/\psi$ production cannot, at present, be used to discriminate models of nuclear gluon distributions.

## V. THE NUCLEAR DRELL-YAN PROCESS

In this section we consider reactions in which a high-energy proton collides with a nucleus and produces a pair of oppositely charged leptons (Drell-Yan process, Fig. 1) leading to lepton pairs of high mass. For an excellent review see Kenyon.[73]

The $\rho$, $\psi$, and $\Upsilon$ families of resonances stand out clearly in the Drell-Yan process, and the search for other resonances is still a strong motivation for these experiments.[74] However, the underlying continuum is our concern here. Drell and Yan[31] argued that the continuum of $\mu^+\mu^-$ pairs produced in hadron-hadron collisions is due to the quark-antiquark annihilation process of Fig. 1.

The computed cross sections for lepton-pair production depend on the longitudinal momentum distributions of quarks and antiquarks. This feature has been exploited to determine structure functions. For example, the Drell-Yan process is the primary source of information regarding the structure functions of mesons.[75]

Another possible application of the Drell-Yan process is the determination of the nuclear quark and antiquark distributions.[23,31,64,71,76] The antiquark distributions are of most interest here, since the different models of the EMC effect necessarily have similar quark distributions, but the nuclear antiquark distributions given by the model can differ significantly.

### A. Drell-Yan reaction mechanism

The property that allows the determination of structure functions from the Drell-Yan process is the so-called "factorization theorem."[77] This means that the Drell-Yan cross section can be calculated as a convolution of parton structure functions, which include the effects of soft gluons, with hard-scattering amplitudes represented by diagrams of perturbative QCD (Ref. 78).

The double-differential Drell-Yan (DY) cross section takes the form [see Eqs. (117) and (126) of Altarelli, Ellis, and Martinelli[78]]:

$$\frac{d^2\sigma}{dM^2dy}=\sum_{a,b}\int\frac{d\xi_1}{\xi_1}\frac{d\xi_2}{\xi_2}f_a^P(\xi_1,Q^2)H_{ab}\left[\frac{x_1}{\xi_1},\frac{x_2}{\xi_2},Q^2\right]\times f_b^T(\xi_2,Q^2)\,, \tag{5.1}$$

where the $a,b$ sums go over parton types $(q,\bar{q},g)$. The $f$'s are parton distribution functions in the projectile ($P$) and target ($T$). The functions $H$ are the hard-scattering amplitudes. In (5.1) $M$ denotes the total mass of the lepton pair (in its rest frame). Since the total four-momentum of the lepton pair is equal to that of the virtual photon $Q^\mu$, we have $M^2=Q^2$. The quantity $y$ is the longitudinal rapidity of the lepton pair:

$$y=\frac{1}{2}\ln\left[\frac{Q^0+Q^3}{Q^0-Q^3}\right]. \tag{5.2}$$

The quantities $x_1$ and $x_2$ are related to these by

$$x_1=e^y\left[\frac{M^2}{s}\right]^{1/2},\quad x_2=e^{-y}\left[\frac{M^2}{s}\right]^{1/2}, \tag{5.3}$$

where $s$ is the square of the total four-momentum of the projectile and one of the target nucleons. Other kinematic quantities which are often used in studying DY data are

$$\tau=\frac{M^2}{s}=x_1x_2,\quad x_F=x_1-x_2\,. \tag{5.4}$$

The factorized form is remarkable: it says that the proton-nucleus DY process is not influenced by initial-state interactions. The physical basis for this result is the high speed of the proton. If the time required for the incident proton to pass through the nucleus is small compared to natural times in the proton's rest frame, then the proton wave function cannot be influenced until long after the hard DY process takes place. This argument is initially due to Landau and Pomeranchuk.[79] However, there are limitations on its validity.[80,81] In particular, if the nucleus were infinitely large, the time available for the proton to interact with the target would be infinitely long and initial-state interactions would invalidate the impulse approximation. The target-length condition necessary for the validity of Eq. (5.1) requires that[80]

$$Q^2\gg m_NL\mu^2\xi_2\,, \tag{5.5}$$

where $m_N$ is the nucleon mass, $L$ is the length of the target nucleus, and $\mu$ is a typical hadronic mass on the order of 350 MeV. For Fe, $L\simeq 2\times(1.1\times 56^{1/3})$ fm and the condition becomes

$$Q^2\gg(4\ \text{GeV}^2)\xi_2\,. \tag{5.6}$$

This is easy to satisfy. See also Ref. 81.

The QCD formula (5.1) is very successful[77] in describing recent Drell-Yan data produced at low and high transverse momentum at the CERN ISR. To apply Eq. (5.1) the only requirements are parton densities extracted from experiments, and an acceptable value for the QCD $\Lambda$ parameter.

Before discussing the nuclear applications of this process, we describe an approximation to the DY cross section which is more usually used than the full QCD expression (5.1). The results of Altarelli, Ellis, and Martinelli indicate that, over a fairly wide kinematic range, the cross section can be well approximated by an expression with the same form as in the naive parton model:

$$\frac{d^2\sigma}{dM^2dx_F}=\frac{4\pi\alpha^2}{9M^4}\left[\frac{x_1x_2}{x_1+x_2}\right]\times K\sum_a e_a{}^2[q_a^P(x_1,Q^2)\bar{q}_a^T(x_2,Q^2)+\bar{q}_a^P(x_1,Q^2)q_a^T(x_2,Q^2)]\,, \tag{5.7}$$

where the sum on $a$ runs over all flavors of quarks in the target. If the naive parton model were correct, $K$ would be unity. The QCD corrections lead to a $K$ which is approximately equal to 2. This approximation is valid provided that $\tau$ is less than about 0.5, and that the transverse momentum of the lepton pairs is not too large. Under these conditions the full cross section can be written in the form (5.7), and the dependence of $K$ on the kinematics can be neglected. For ratios of cross sections the errors introduced by using this approximation are even smaller. The bulk of our results are therefore given using the parton-model expression (5.7). However, some results of calculations using the complete cross section of Altarelli, Ellis, and Martinelli are presented below.

Our aim is to use the various models of quark distribution functions in the nucleus to compute the DY cross section. The expression (5.7) depends on a different combination of structure functions than that measured in DIS. In particular, experiments can separate the term in which a target antiquark is annihilated by making measurements for fairly large values of $x_1$ for which the projectile sea is essentially absent, thus providing information about the target ocean.[32]

It is worth emphasizing here that we advocate the use of proton beams. Pion beams contain valence antiquarks, so there is no kinematic regime sensitive to the target antiquark distributions.

### B. Nuclear calculations

Searches for nuclear dependence of parton structure functions have been carried out.[73] If the impulse approximation were valid, the nuclear DY cross section would be proportional to the number of nucleons, $A$. Indeed the $A$ dependence of the cross section $d\sigma/dM$ is well approximated by a linear form when $M$ is large enough, as shown in Fig. 16(a) of Ref. 73. If the $A$ dependence of $d\sigma/dM$ is parametrized by $A^\alpha/\alpha$ is essentially unity for $M>5$ GeV. For small masses $d\sigma/dM$ is proportional to $A^{2/3}$ as expected from nuclear shadowing. These data indicate that the dominant effect of the target nucleus is to provide $A$ nucleons. We propose using the double-differential cross section $d^2\sigma/dM\,dy$ to look for an $A$ dependence similar to that seen in DIS. In certain kinematic regions nuclear effects do stand out.[32]

Our procedure is to study and compare the nuclear Drell-Yan cross sections predicted by each of the different classes of models. For ease of comparison with earlier sections we shall continue here to show results for the nuclei Fe and D.

One can first work at small $x_1$ to see that the ratios of Fe to D Drell-Yan cross sections reproduce the trends seen in DIS. That this is indeed the case is shown in Ref. 32. The pattern of enhancement at low $x_2$ and depletion at medium $x_2$ is reproduced in all of the models.

The target sea dominates at large $x_1$, and there one anticipates significant differences between the models. The essential results are displayed in Fig. 13 in which comparisons between the various models are made. Up to five different sets of distribution functions are used for each model.

It is worthwhile to discuss the kinematics used in making the computations of Fig. 13. The ratios shown are evaluated at a fixed value of $Q^2$ ($Q^2=50$ GeV$^2$). The relation $Q^2/s=x_1x_2$ indicates that the proton's laboratory energy varies from about 1330 to 380 GeV as $x_2$ ranges between 0.2 and 0.7. This huge range of beam energies is very difficult to obtain. However there is another way to look at these plots. We deal with ratios, and these are almost independent of $Q^2$. Varying the fixed value of $Q^2$ between 25 and 200 GeV$^2$ changes none of the parton-model ratios by more than about 2%. Thus the results of Fig. 13 as well as the figures given below can also be viewed as ratios obtained as fixed laboratory energy, cf. Sec. V D below.

To organize the discussion of Fig. 13, first compare the different models using one structure function set, say DO1. *Especially noteworthy is that each of the different models presents curves with very different shapes.* Huge differences between the models are apparent. Results are shown for $x_1=0.7$, but very similar results are obtained for $x_1=0.5$. We next discuss some specific points.

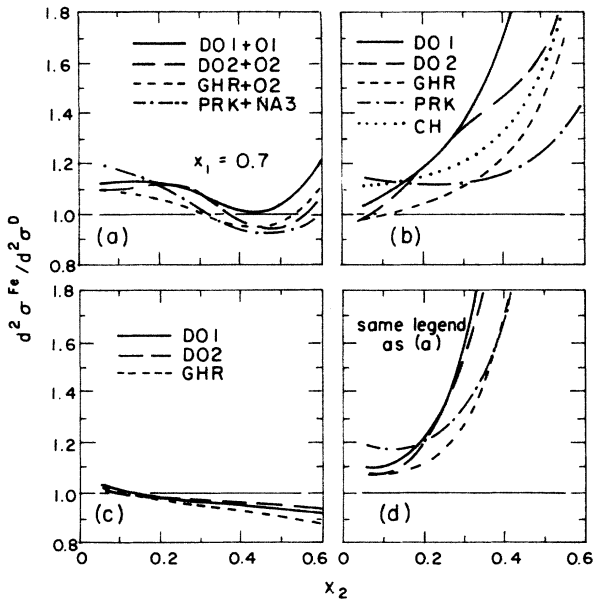


FIG. 13. Drell-Yan cross-section ratios for Fe to D at $x_1=0.7$ with differing choices of quark distributions in D: (a) Ericson-Thomas pion model; (b) Carlson-Havens six-quark model; (c) dynamical rescaling; (d) pion model of Berger, Coester, and Wiringa. Momentum-dependent distributions are evaluated at $Q^2=50$ GeV$^2$.

The two pion enhancement models lead to very different DY results. The Ericson-Thomas approach gives an $f_\pi(y)$ which is large only for $y<0.3$ (Fig. 3). Hence the enhancement of ocean quarks is limited to small values of $x_2$. This model can lead to some ocean enhancement for all values of $x_2$. This occurs when a bag radius $R$ of about 0.8 fm or larger is used. [For smaller values of $R$, there are more excess pions and less momentum carried by the nucleons, so one sees an enhancement for $x_2<0.2$ and a depletion for $x_2>0.3$ (Ref. 32).] In contrast, the excess-pion distribution of Berger, Coester, and Wiringa extends to momenta greater than $m_N$. This leads to huge enhancements of the Drell-Yan cross section for heavy nuclei.

Now consider the six-quark cluster model. The explicit functional dependence on $x_2/2$, Sec. III, leads to an enhancement of $\bar{q}^T(x_2)$ for values of $x_2$ greater than about 0.2.

Dynamical rescaling predicts a modification of the antiquark distribution function. One employs $\bar{q}(x,\xi Q^2)$ instead of $\bar{q}(x,Q^2)$. This changes the DY cross section per nucleon in heavy nuclei, but not by much. Typical values of the ratio $\bar{q}(x,\xi Q^2)/\bar{q}(x,Q^2)$ are a 3% increase at small $x$ and a 5% decrease at large $x$. This small sensitivity is caused by the slow, logarithmic variation of the distribution functions. Small changes are therefore expected in heavy nuclei, as are seen in Fig. 13.

Next consider the sensitivity of our results to the choice of pion and nucleon structure functions. For the nucleon we have used the two parameter sets given by Duke and Owens, as well as that of Gluck, Hoffman, and Reya and the BEBC parametrizations of Parker *et al.*; for the pion we have used the NA3 results and the $Q^2$-dependent fits of Owens. There are some minor quantitative differences in the results, as shown in Fig. 13. The qualitative features of the results are independent of the choice of structure functions. However, the pion-enhancement model of Berger, Coester, and Wiringa and the six-quark cluster model are much more sensitive to these variations than the other models. In the large-$x_2$ region of interest, this is because the significantly enhanced values of $\bar{q}^T(x_2)$ make the ratio sensitive to variations, rather than because of actual variations.

The very clear result of all of these considerations is that models with very similar nuclear DIS predict very different lepton-pair production rates. Thus, one can reasonably hope that an accurately done Drell-Yan experiment could distinguish the different models.

### C. Experimental questions

It is worthwhile to ask if an experiment which compares $d^2\sigma/dM^2dx_F$ for a light and heavy nucleus has ever been done. In our survey of the literature it seems possible that experiments could have measured and compared $d^2\sigma/dM^2dx_F$ for different nuclei but the only published results are for single-differential cross sections. A detailed nuclear comparison of the double-differential cross

section has not been made.

Another question is "can the experiment be done?" It is helpful to consider existing data. The double-differential cross-section data from the 1980 experiment by the Columbia-Fermilab—Stony Brook (CFS) Collaboration[62] is shown in Fig. 14(a) of Ref. 63. The kinematic region that we require is $x_2 \sim 0.4$—$0.5$ with rapidity, $y > 0$. That figure shows that the cross section of interest is not too small. Our special region was of no particular interest to those experimentalists and the error bars were fairly large—typically 20%, although some as small as 5% appear. While a dedicated experiment ought to be able to do better, the fact still remains that this data is for PT and we desire a light nucleus for comparison. For such a nucleus, the statistics could be worse. However, notwithstanding these experimental errors, the CFS group claim to be able to extract antiquark distributions in Pt with very high accuracy, as shown in Fig. 14. This is possible by using information from DIS on the quark distributions in the proton beam.

Also shown in Fig. 14 is the momentum distribution of the ocean extracted by the Michigan-Northeastern-Tufts-Washington (MNTW) Collaboration from their DY data[64] on W. The uncertainty in the MNTW fit is comparable to that of CFS and the respective fits are consistent with each other. Note that both curves should be lowered by an appropriate $K$ factor. The presence of this factor is primarily responsible for the discrepancy, visible at low $x$, with data on the ocean extracted from neutrino experiments[82,83] on Fe. To our knowledge, no neutrino experiment has been able to extract useful nonzero results for the ocean distributions for $x$ values as large as has been managed by the DY experiments. Except for very small values of $x$, where antineutrino DIS is most useful, Drell-Yan seems to be the best way to determine antiquark distributions. Thus a DY experiment dedicated to seeing nuclear effects could determine important information regarding nuclear parton distributions. The requirements will be high statistics, very good control of systematic errors, and data for large rapidity.

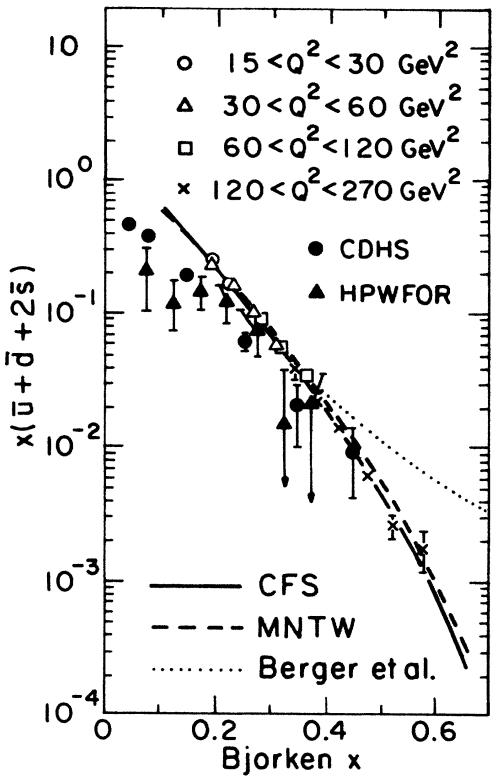


FIG. 14. Ocean distributions extracted from DY experiments on Pt (solid curve) by the CFS collaboration (Ref. 63), and W (dashed curve) by the MNTW collaboration (Ref. 64). The data points for various $Q^2$ bins are those of the CFS collaboration. They are compared with data extracted by the CDHS (Ref. 82) HPWFOR (Ref. 83) collaborations. Also shown is the prediction of the pion model of Berger, Coester, and Wiringa at $Q^2 = 100$ GeV$^2$.

Even if accurate data on light nuclei are difficult to obtain, any information on the ocean distribution for heavy nuclei would still be of interest as the following example illustrates. Also shown in Fig. 14 is the prediction of the model of Berger, Coester, and Wiringa. Because the pionic contribution to the ocean in the region $0.4 < x < 0.6$ is several times larger in this model than the nucleonic contribution (which is strongly depleted), this prediction is not sensitive to our poor knowledge of the free nucleon ocean. As can be seen the disagreement with data is marked. Thus structure functions extracted from DY data can already eliminate a model which is compatible with all other data. Berger[47] has argued that the CFS extraction of the antiquark distribution requires the model-dependent assumptions that the cross section is linear in $A$ for all $x_1$ and $x_2$ and, that the quark distribution is taken from CDHS. However, we believe that these effects of such assumptions are too small to cure the order-of-magnitude discrepancy evident displayed in Fig. 14. Note that the DY curves are actually $Kx\bar{q}(x)$ whereas the curve labeled Berger *et al.* is just $x\bar{q}(x)$.

### D. QCD corrections

Our purpose here is to study the influence of the leading-order QCD corrections in Eq. (5.1), and to verify that the model differences displayed in Fig. 13 persist. The gluon-Compton terms of Ref. 78 provide a contribution that we have not incorporated above. We find that only minor variations (never greater than about 4%) are obtained.

First, consider DY ratios of Fe to D cross sections for the QCD expression of Altarelli, Ellis, and Martinelli (5.1) and the parton model. Recall that the most significant QCD corrections are incorporated in the $K$ factor of Eq. (5.7). Since we consider ratios, the $K$ factor drops out if (5.7) is used, but not with (5.1). We call the formalism of (5.1) "QCD corrected." The one of (5.7) is denoted by "parton model," even though QCD effects change the

strength of the cross section.

For small $x_1$, the QCD corrections do not change the DY ratios in any observable way. This is expected, since the valence quarks of the target dominate. The rescaling (with DO2) and Ericson-Thomas pion models are used. (No one knows the scaling violations of a six-quark bag.) Our numerical results are for fixed laboratory proton energy.

For $x_1=0.7$ there is some very small influence of the QCD corrections, see Fig. 15. The DY ratios for fixed $s$ are similar to those at fixed $Q^2$. The QCD effects are largest for the smaller beam energy, which for fixed $x_1x_2$ corresponds to smaller values of $Q^2$ and larger values of $\alpha(Q^2)$. The large value of $\Lambda$ employed in DO2 leads to larger (by about a factor of 2) QCD effects than would be obtained with DO1. These days the smaller value of 200 MeV is preferred.

The influence of QCD corrections can be neglected unless the DY experiment is done at low beam energy, and a large value of $\Lambda$ is required to describe scaling violations.

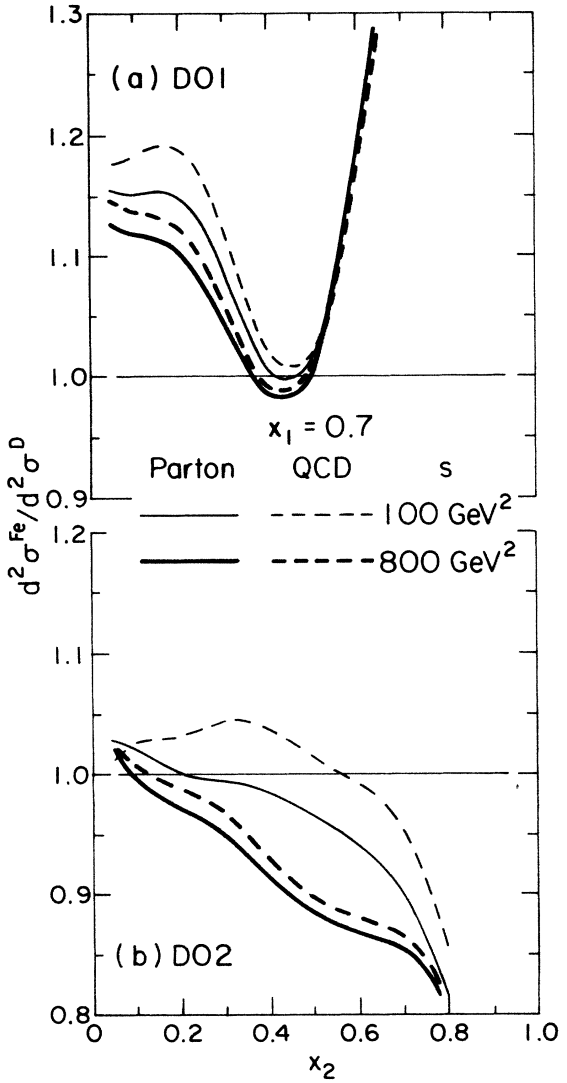


FIG. 15. QCD corrections to the ratio of DY cross sections in Fe to D at $x_1=0.7$ for two proton beam energies. QCD-corrected (dashed curve) vs "parton model" (solid curve): (a) Ericson-Thomas pion model; (b) dynamical rescaling.

## VI. SUMMARY

A detailed study of the models of the EMC effect reveals that each has significant flaws or uncertainties. For example, all of the models are very sensitive to the choice of free nucleon structure function. The six-quark cluster model (Fig. 5) has huge variations at $x \lesssim 0$. The dynamical rescaling gives a structure function ratio (Fig. 7) that passes through unity at $x=0.1$ if conventional structure functions (e.g., Refs. 40 and 41) are used. This is in contrast with the CRR result of $\sim 0.2$ obtained with their own function. The pionic models depend on imprecisely known parameters. The model of Berger, Coester, and Wiringa is in conflict with antiquark distributions (Fig. 14) extracted from Drell-Yan and other data.

Nevertheless, we find that each model has characteristic features, and most of the present paper is concerned with determining the experiments that illuminate these.

Natural processes to consider are neutrino and antineutrino DIS on nuclei which enables one to extract separate valence and ocean distributions. However, most models make similar predictions for the valence distribution at small $x$, and all the models we have examined are unreliable in this experimentally difficult region. In contrast we have found substantial qualitative differences between various predictions for the ocean at intermediate $x$ ($\gtrsim 0.3$). Unfortunately, the ocean is dying out in this region and current prospects for measuring the tail of the ocean distribution with antineutrinos do not seem bright. Thus, the (anti)neutrino data do not distinguish the models.

The process of $J/\psi$ production in muon-nucleus collisions, which is a possible means to determine the nuclear gluon distribution, is also considered. There are uncertainties in the free-nucleon gluon distribution function, as well as in the knowledge of the mechanism for $J/\psi$ formation. The data is also limited to very low values of $x$. Thus this interesting process is not yet very useful in separating the models.

The Drell-Yan lepton-pair production in proton-nucleus collisions is in our view the process with the best prospects for determining unknown aspects of nuclear parton distributions. For the experimentally accessible kinematic regions in which the annihilation of a projectile quark and a target antiquark dominate, the characteristic features of the predicted nuclear ocean distributions lead to very different DY production cross sections in the various models. Depending on the model parameters, the pion enhancement effect gives slight decreases or slight increases to the nuclear DY cross section per nucleon. The six-quark cluster model predicts huge increases, while dynamical rescaling predicts small decreases. Moreover, the shapes of the double-differential cross sections are

very different for each of the models, Fig. 13. These qualitative features are not changed by using different input data such as different parton distributions of the free nucleon. Furthermore, QCD effects such as the gluon-quark Compton scattering processes do not significantly change the predicted ratios of nuclear (per nucleon) to nucleon DY cross sections.

## ACKNOWLEDGMENTS

We would like to thank F. Close, F. Coester, R. Jaffe, B. McKellar, R. Roberts, D. Soper, and A. Thomas for useful discussions. This work was supported in part by the U.S. Department of Energy.

*Present address: Physics Department, University of Adelaide, G.P.O. Box 498 Adelaide, South Australia 5001.

†Present address: Department of Theoretical Physics, Schuster Laboratory, University of Manchester, Manchester, M13 9PL, U.K.

[1]J. J. Aubert *et al.*, Phys. Lett. **123B**, 275 (1983).

[2]A. W. Thomas, Adv. Nucl. Phys. **13**, 1 (1983); G. A. Miller, *Quarks and Nuclei,* edited by W. Weise (World Scientific, Singapore, 1984), Vol. 1.

[3]A. Bodek *et al.*, Phys. Rev. Lett. **50**, 1431 (1983).

[4]A. Bodek *et al.*, Phys. Rev. Lett. **51**, 534 (1983).

[5]R. G. Arnold *et al.*, Phys. Rev. Lett. **52**, 727 (1984).

[6]A. C. Benvenuti *et al.*, in *Proceedings of the 22nd International Conference on High Energy Physics, Leipzig, 1984,* edited by A. Meyer and E. Wieczorek (Akademie der Wissenschaften der DDR, Zeuthen, East Germany, 1984), Vol. 1, p. 219; G. Bari *et al.*, Phys. Lett. **163B**, 282 (1985).

[7]M. A. Parker *et al.*, Nucl. Phys. **B232**, 1 (1984).

[8]A. E. Asratyan *et al.*, Serpukhov Report No. ITEP-110, 1983 (unpublished); V. V. Ammosov *et al.*, Zh. Eksp. Teor. Fiz. **39**, 327 (1984) [JETP Lett. **39**, 393 (1984)].

[9]A. M. Cooper *et al.*, Phys. Lett. **141B**, 133 (1984).

[10]H. Abramowicz *et al.*, Z. Phys. C **25**, 29 (1984).

[11]C. H. Llewellyn Smith, Phys. Lett. **128B**, 107 (1983).

[12]M. Ericson and A. W. Thomas, Phys. Lett. **128B**, 112 (1983).

[13]M. Ericson, in *Mesons, Isobars, Quarks, and Nuclear Excitations,* proceedings of the International School of Subnuclear Physics, Erice, 1983 [*Progress in Particle and Nuclear Physics,* edited by D. Wilkinson (Pergamon, London, 1984), Vol. 11]; Prog. Part. Nucl. Phys. **11**, 277 (1984).

[14]A. W. Thomas, in *Mesons, Isobars, Quarks, and Nuclear Excitations* (Ref. 13); Prog. Part. Nucl. Phys. **11**, 325 (1984).

[15]E. L. Berger, F. Coester, and R. B. Wiringa, Phys. Rev. D **29**, 398 (1984).

[16]R. L. Jaffe, Phys. Rev. Lett. **50**, 228 (1983).

[17]C. E. Carlson and T. J. Havens, Phys. Rev. Lett. **51**, 261 (1983).

[18]H. J. Pirner and J. Vary, University of Heidelberg Report No. UNI-HE-83-02, 1983 (unpublished); J. P. Vary, Nucl. Phys. **A418**, 195c (1984); H. J. Pirner and J. P. Vary, Phys. Rev. Lett. **46**, 1376 (1981).

[19]S. Date, Prog. Theor. Phys. **70**, 1682 (1983).

[20]M. Chemtob and R. Peshanski, J. Phys. G **10**, 599 (1984).

[21]B. C. Clark *et al.*, Phys. Rev. D **31**, 617 (1985).

[22]L. A. Kondratyuk and M. Zh. Shmatikov, Z. Phys. A **321**, 301 (1985).

[23]G. Berlad, A. Dar, and G. Eilam, Phys. Rev. D **22**, 1547 (1980).

[24]F. E. Close, R. G. Roberts, and G. G. Ross, Phys. Lett. **129B**, 346 (1983).

[25]R. L. Jaffe *et al.*, Phys. Lett. **134B**, 449 (1984).

[26]F. E. Close *et al.*, Phys. Rev. D **31**, 1004 (1985).

[27]O. Nachtmann and H. J. Pirner, Z. Phys. C **21**, 277 (1984); G. Chanfray, O. Nachtmann, and H. J. Pirner, Phys. Lett. **147B**, 249 (1984).

[28]N. N. Nikolaev and V. I. Zakharov, Phys. Lett. **55B**, 397 (1975); L. L. Frankfurt and M. I. Strikman, Leningrad Nuclear Physics Institute Report No. 886, 1983 (unpublished).

[29]For example, H. Faissner and B. R. Kim, Phys. Lett. **130B**, 321 (1983).

[30]J. J. Aubert *et al.*, Phys. Lett. **152B**, 428 (1985).

[31]S. D. Drell and T. M. Yan, Phys. Rev. Lett. **25**, 316 (1970); **24**, 181 (1970); Ann. Phys. (N.Y.) **66**, 578 (1971).

[32]R. P. Bickerstaff, M. C. Birse, and G. A. Miller, Phys. Rev. Lett. **53**, 2532 (1984).

[33]S. J. Wimpenny, Nucl. Phys. **A434** (1985).

[34]G. V. Dunne and A. W. Thomas, Phys. Rev. D **33**, 2061 (1986); S. V. Akulinichev, S. A. Kulagin, and G. M. Vagradov, Phys. Lett. **158B**, 485 (1985); R. P. Bickerstaff and G. A. Miller, Phys. Lett. B (to be published); S. K. Akulinichev, S. Shlomo, S. A. Kulagin, and G. M. Vagradov, Phys. Rev. Lett. **55**, 2239 (1985).

[35]C. H. Llewellyn Smith, Nucl. Phys. **A434**, 35c (1985).

[36]S. Théberge, A. W. Thomas, and G. A. Miller, Phys. Rev. D **22**, 2838 (1980); **23**, 2106(E) (1981); A. W. Thomas, S. Théberge, and G. A. Miller, *ibid.* **24**, 216 (1981).

[37]E. Oset *et al.*, Phys. Rep. **C83**, 281 (1982); A. B. Migdal, Rev. Mod. Phys. **50**, 107 (1978).

[38]E. J. Moniz *et al.*, Phys. Rev. Lett. **26**, 445 (1971).

[39]R. L. Jaffe, Comments Nucl. Part. Phys. **13**, 39 (1984).

[40]D. W. Duke and J. F. Owens, Phys. Rev. D **30**, 49 (1984).

[41]M. Gluck, E. Hoffman, and E. Reya, Z. Phys. C **13**, 119 (1982).

[42]For the parameter $\gamma$ describing the ocean we use the updated value from M. Jonker *et al.*, Phys. Lett. **128B**, 117 (1983).

[43]J. F. Owens, Phys. Rev. D **30**, 943 (1984).

[44]J. Badier *et al.*, Z. Phys. C **18**, 281 (1983).

[45]A. W. Thomas, Hadron Physics at Intermediate Energies, proceedings of Regensburg Workshop, 1984, edited by W. Weise (unpublished), p. 293. This and Ref. 46 cite work in progress by Ericson, Llewellyn Smith, and Thomas.

[46]A. W. Thomas, in *Proceedings of the International Conference on Nuclear Physics* (On the Occasion of the Golden Jubilee of the Indian Natural Science Academy), Bombay, 1984, edited by B. K. Jain and B. C. Sinha (World Scientific, Singapore, 1985).

[47]E. L. Berger and F. Coester, Phys. Rev. D **32**, 1071 (1985); E. L. Berger, Nucl. Phys. **B267**, 231 (1986).

[48]B. L. Friman, V. R. Pandharipande, and R. B. Wiringa, Phys. Rev. Lett. **51**, 763 (1984).

[49]See, e.g., *Hadron Substructure in Nuclear Physics,* edited by W.-Y. P. Hwang and M. H. Macfarlane (AIP Conf. Proc. No.

110) (AIP, New York, 1984).
[50]See the review, e.g., D. Sivers, Ann. Rev. Nucl. Part. Sci. **32**, 149 (1982).
[51]D. J. Gross and F. Wilczek, Phys. Rev. D **9**, 980 (1974); H. D. Politzer, Phys. Rep. **14C**, 129 (1974); S. Brodsky and J. Gunion, Phys. Rev. D **19**, 1005 (1979).
[52]J. M. Greben and A. W. Thomas, Phys. Rev. C **30**, 1021 (1984).
[53]R. L. Jaffe and G. G. Ross, Phys. Lett. **93B**, 313 (1980).
[54]A. W. Hendry, D. B. Lichtenberg, and E. Predazzi, Phys. Lett. **136B**, 433 (1984).
[55]M. Jandel and G. Peters, Phys. Rev. D **30**, 1117 (1984).
[56]L. S. Celenza, A. Rosenthal, and C. M. Shakin, Phys. Rev. Lett. **53**, 892 (1984).
[57]C. J. Horowitz, E. J. Moniz, and J. W. Negele, Phys. Rev. D **31**, 1689 (1985).
[58]G. Altarelli and G. Parisi, Nucl. Phys. **B126**, 298 (1977).
[59]M. Bace, Phys. Lett. **78B**, 132 (1978).
[60]E. Eichten, I. Hinchcliffe, K. Lane, and C. Quigg, Rev. Mod. Phys. **56**, 579 (1984); J. G. Morfin and J. F. Owens, Report No. FERMILAB-Conf-85/15, 1985 (unpublished).
[61]J. J. Aubert *et al.*, Phys. Lett. **123B**, 123 (1983).
[62]H. Abramowicz *et al.*, Z. Phys. C **17**, 283 (1983).
[63]CFS Collaboration, C. Ito *et al.*, Phys. Rev. D **23**, 604 (1981).
[64]MNTW collaboration, S. R. Smith *et al.*, Phys. Rev. Lett. **46**, 1607 (1981).
[65]M. Ericson and A. W. Thomas, Phys. Lett. **148B**, 191 (1984).
[66]H. Wahlen, in *Gluons and Heavy Flavours,* proceedings of the 18th Rencontre de Moriond, 1983, edited by J. Tran Thanh Van (Editions Frontières, Gif-sur-Yvette, 1983), p. 13.
[67]See, for example, V. Barger, W. Y. Keung, and R. J. N. Phillips, Phys. Lett. **91B**, 253 (1980), and references therein.
[68]EMC Collaboration, J. J. Aubert *et al.*, Nucl. Phys. **B213**, 1 (1983); **B213**, 31 (1983).
[69]R. Ruckl and R. Baier, in *New Flavours,* proceedings of the 2nd Moriond Workshop, 1982, edited by J. Tran Thanh Van (Editions Frontières, Gif-sur-Yvette, 1982); see also R. Baier and R. Ruckl, Nucl. Phys. **B218**, 289 (1983).
[70]J. Owens, in *New Flavours* (Ref. 69).
[71]Owens (Ref. 43), and references therein.
[72]F. E. Close, R. G. Roberts, and G. G. Ross, Z. Phys. C **26**, 515 (1985).
[73]I. R. Kenyon, Rep. Prog. Phys. **45**, 1261 (1982).
[74]J. Rutherfoord (private communication, Fermilab Experiment E605).
[75]C. B. Newman *et al.*, Phys. Rev. Lett. **42**, 951 (1979); M. J. Corden *et al.*, Phys. Lett. **96B**, 417 (1980); R. Barate *et al.*, Phys. Rev. Lett. **43**, 1541 (1979); J. Badier *et al.* (Ref. 66).
[76]K. V. L. Sarma, Phys. Rev. D **22**, 216 (1980); S. Date and A. Nakamura, Prog. Theor. Phys. **69**, 565 (1983); R. M. Godbole and K. V. L. Sarma, Phys. Rev. D **25**, 120 (1982).
[77]J. C. Collins, D. E. Soper, and G. Sterman, Phys. Lett. **109B**, 388 (1981); Nucl. Phys. **B223**, 381 (1983); Phys. Lett. **134B**, 263 (1984); P. V. Landsdhoff and W. J. Stirling, Z. Phys. C **14**, 251 (1981); W. W. Lindsay, D. A. Ross, and C. T. Sachrajda, Nucl. Phys. **B214**, 61 (1983); A. Sen and G. Sterman, *ibid.* **B229**, 231 (1983); J. C. Collins, D. E. Soper, and G. Sterman, University of Oregon Report No. OITS 287, 1985 (unpublished); G. T. Bodwin, Phys. Rev. D **31**, 2616 (1985).
[78]G. Altarelli, R. K. Ellis, and G. Martinelli, Nucl. Phys. **B157**, 461 (1979).
[79]L. Landau and I. Pomeranchuk, Dokl. Akad. Nauk SSSR **92**, 535 (1953) [Sov. Phys. Dokl. **92**, 735 (1953)].
[80]G. T. Bodwin, S. J. Brodsky, and G. P. Lepage, Report No. SLAC-PUB-2927, 1982 (unpublished); S. J. Brodsky, in *Workshop for Heavy Flavors,* proceedings of the 3rd International Conference on Physics in Collision, Como, 1983, edited by G. Bellini, A. Bettini, and L. Perasso (Editions Frontières, Gif-sur-Yvette, France, 1984), p. 93.
[81]A. Mueller, in *New Flavors* (Ref. 69).
[82]CDHS Collaboration, J. D. H. de Groot *et al.*, Z. Phys. C **1**, 143 (1979).
[83]Harvard - Pennsylvania - Wisconsin - Fermilab - Ohio - Rutgers (HPWFOR) Collaboration, A. Benvenuti *et al.*, Phys. Rev. Lett. **42**, 1317 (1979).